MASCOT - The Mobile Asteroid Surface Scout onboard the Hayabusa2 Mission

Tra-Mi Ho[1], Volodymyr Baturkin[1], Ross Findlay, Christian Grimm[1], Jan Thimo Grundmann[1], Catherin Hobbie[1], Eugen Ksenik[1], Caroline Lange[1], Kaname Sasaki[1], Markus Schlotterer[1], Maria Talapina[1], Nawarat Termtanasombat[1], Elisabeth Wejmo[1], Lars Witte[1], Michael Wrasmann[1], Guido Wübbels[1], Johannes Rößler, Christian Ziach[1], Jens Biele[2], Christian Krause[2], Stephan Ulamec[2], Michael Lange[3], Olaf Mierheim[3], Roy Lichtenheldt[4], Maximilian Meier[4], Josef Reill[4], Hans-Jürgen Sedlmayr[4], Pierre Bousquet[5], Anthony Bellion[5], Olivier Bompis[5], Celine Cenac-Morthe[5], Muriel Deleuze[5], Stephane Fredon[5], Eric Jurado[5], Elisabet Canalias[5], Ralf Jaumann[6], Jean-Pierre Bibring[7], Karl Heinz Glassmeier[8], David Hercik[8], Matthias Grott[6], Luca Celotti[9], Federico Cordero[10], Jeffrey Hendrikse[11], Tatsuaki Okada[12].

[1]*DLR (German Aerospace Center), Institute of Space Systems, Robert-Hooke-Str. 7, 28359 Bremen, Germany*

[2]*DLR, Space Operations and Astronaut Training, MUSC, Linder Höhe, 5147, Köln, Germany*

[3]*DLR, Institute of Composite Structures and Adaptive Systems, Lilienthalplatz 7, 38108 Braunschweig, Germany*

[4]*DLR, Robotic and Mechatronics Center, Münchener Straße 20,82234 Oberpfaffenhofen-Wessling, Germany*

[5]*CNES, 18 Avenue Edouard Belin, 31400 Toulouse, France*

[6]*DLR, Institute of Planetary Research, Rutherfordstrasse 2, 12489 Berlin-Adlershof, Germany*

[7]*IAS, Université Paris Sud - Bat 121, 91405 ORSAY CEDEX, France*

[8]*Technische Universität Braunschweig, Mendelssohnstraße 3, 38106 Braunschweig, Germany*

[9] *Active Space Technologies GmbH, Carl-Scheele-Strasse 14, 12489 Berlin*

[10] *Telespazio-Vega, Europaplatz 5, 64293 Darmstadt, Germany*

[11] *Airbus DS, 88039 Friedrichshafen, Germany*

[12] *ISAS/JAXA, 3-1-1 Yoshinodai, Sagamihara, JAPAN*

[1]Phone: +49-421-244201171

[1]Fax: +49-421-244201124

[1] Email: Tra-Mi.Ho@dlr.de

Abstract

On December 3rd, 2014, the Japanese Space Agency (JAXA) launched successfully the Hayabusa2 (HY2) spacecraft to its journey to Near Earth asteroid (162173) Ryugu. Aboard this spacecraft is also a compact landing package, MASCOT (Mobile Asteroid surface SCOuT), which was developed by the German Aerospace Centre (DLR) in collaboration with the Centre National d'Etudes Spatiales (CNES). Similar to the famous predecessor mission Hayabusa, Hayabusa2, will also study an asteroid and return samples to Earth. This time, however, the target is a C-type asteroid which is considered to be more primitive than 25143 Itokawa and provide insight into an even earlier stage of our Solar System.

Upon arrival at the asteroid in 2018, MASCOT will be released from the HY2 spacecraft and gently descend by free fall from an altitude of about 100 m to the surface of the asteroid. After a few bounces, the lander will come to rest at the surface and start to perform its scientific investigations of the surface structure, mineralogical composition, thermal behavior and magnetic properties by operating its four scientific instruments. Those include an IR imaging spectrometer (MicrOmega, IAS Paris), a camera (MASCAM, DLR Berlin), a radiometer (MARA, DLR Berlin) and a magnetometer (MASMAG, TU Braunschweig).

In order to allow optimized payload operations an optimized thermal design is required to cope with the contrasting requirements of the 4-year cruise in cold environment versus the hot conditions on the surface of the asteroid. Operations up to 2 asteroid days (~16 hours) based on a primary battery are currently envisaged. A mobility mechanism allows locomotion on the surface supported by an attitude and motion sensing system and an intelligent autonomy manager, which is implemented in the onboard Software, which can operate MASCOT when ground intervention is not available.

Keywords: Hayabusa2, MASCOT, surface science packet, asteroid

1 Introduction

The field of minor bodies exploration comprises in the last few decades flyby missions such as Giotto (Reinhard et al. (Nature vol 321 p313, Keller et al., 1986); the flyby and impact mission Deep Impact (A'Hearn et al., 2005b); orbiting and landing missions such as Rosetta (Glassmeier et al., 2007; Sierks et al., 2015) and others to return samples back to Earth like Stardust (Brownlee et al., 2004) and Hayabusa (Fujiwara et al., 2006). They all unveiled a tremendous amount of new insights on the nature of the small bodies in our Solar System.

The missions of the last decades, preceding Hayabusa2, gathered important and often unexpected information on comets and asteroids. Since Galileo, on its way to Jupiter, provided the first ever close up data of an asteroid (951 Gaspra, Veverka et al., 1994), many others asteroids and comets have been visited by spacecraft.

The Deep Impact mission (NASA) provided data from the first 30 – 50m layers and thus conclusion on the interior of a cometary nucleus. The mission design contains two elements, i.e. an impactor (~ 350 kg, v_{impact} = 10,2 km/s) and a flyby spacecraft, arriving at comet 9P/Tempel 1 on July 4th, 2005 to create and observe the formation of a large crater that was predicted to be approximately 25 m deep and 100 m wide (A'Hearn et al., 2005a). Later data analysis of the cratering experiment of the mission gives a final impact crater size between 130 – 220 m indicating a low-density (~ 0.2 to 0.5 g cm^{-3}) and highly porous (90%) surface (Schultz et al., 2007). Further important results fromDeep Impact indicated that although the surface temperatures, colors, albedos, and spectra implies nearly no ice (only restricted to few discrete and small areas) the rapid appearance of large amounts of volatiles in the earliest ejecta implies that ices must be located in shallow and sub-surface sources (Sunshine et al., 2007).

The primary goals of NASA's Stardust mission were to capture samples of comet 81P/Wild2 in January 2004 and return them to Earth for laboratory analysis about 2 years later. The resulting analysis of the collected samples showed that comets contain a mix of materials made by conditions of both "fire and ice" (Brownlee et al., 2004).

Comparing with the Stardust mission that collected dust sampled from the coma during a high velocity fly-by, the Japanese Hayabusa mission slowly approached its target, Near-Earth asteroid 25143 Itokowa, to a distance of about 20 km on September 12, 2005. After a period of reconnaissance operation, the spacecraft transferred to the nominal hovering position at an altitude of about 7 km from the asteroid′s surface and near the sub-Earth point (Fujiwara et al., 2006). The Hayabusa spacecraft carried onboard next to four remote sensing instruments; an imaging camera (Saito et al., 2006), a near-infrared spectrometer, a laser ranging instrument (Abe et al., 2006) and an x-ray fluorescence spectrometer (Okada et al., 2006) also a micro-rover named MINERVA that contains a pair of stereoscopic imaging cameras, one short focal length camera, and thermal probes. The MINERVA rover was released, but unfortunately its landing on the asteroid′s surface was not successful (Yoshimitsu et al., 2006). The Hayabusa mission was highly successful in observing an asteroid remotely, identifying evidence of a rubble-pile structure detecting its exact size (~535 x 294 x 209 m^3) and mass, and revealing its compositional homogeneity (Okada et al., 2006) but also diverse

surface morphology unlike observed at previously explored asteroids (Saito et al., 2006).

Rosetta is the first mission to rendezvous with a comet and investigate it in detail during a large fraction of its orbit around the sun and different phases of activities. The Rosetta spacecraft reached its target, 67P/Churyumov-Gerasimenko in August 2014 after ten years of cruise (Accomazzo et al., 2015). Observations with the ten orbiter instruments allowed a first characterization of nucleus and activity and thus the selection of a landing site for Philae, which successfully landed more than once on November 12th, 2014 (Biele et al 2015).

The lander Philae, in many respects, provided heritage for MASCOT. Although much larger (Philae has a mass of about 100kg and accommodates ten scientific instruments, including a drill, cameras a radar instrument and evolved gas analyzers (Biele and Ulamec 2008)) and was designed for long term operations (batteries and solar generator) many aspects of landing on small bodies are similar for both landers (Ulamec and Biele, 2009, Ulamec *et al*. 2014). Also the instruments aboard MASCOT have heritage with Philae, like MASMAG with ROMAP, MARA with MUPUS-TM, MASCAM with ROLIS and to some extent MicrOmega with CIVA-M. Detailed descriptions of the instruments aboard Philae are given e.g. in Schulz *et al*. (2009)

High quality context science will be achieved by the Hayabusa 2 mission (Tsuda et al., 2013), JAXA's Hayabusa immediate follow-on asteroid sample return mission, which will not only perform, similar to its predecessor, remote sensing of a Near-Earth asteroid (NEA) but will, in addition to Hayabusa's science objective, also carry an impactor that will excavate a crater to enable subsurface sampling; an armada of small landers comprising 3 nano-rovers (Minervas-II1 = Rover1A & Rover 1B and Minerva-II2) and the 10kg MASCOT (**M**obile **A**steroid surface **SCO**u**T**) lander, the subject of this paper. For the first time, this mission will link the three analytical fields: remote sensing, in-situ and sample return. Investigation will be performed at multiple landing sites and thus able to cover a variety of asteroid terrains and retrieve in-depth information on the nature of its target object. MASCOT is an agile, lightweight, highly capable mobile science platform that has been developed by the German Aerospace Centre (DLR) in collaboration with CNES. MASCOT is belonging to the class of nanosatellites and is carrying four

scientific instruments: a camera (MASCAM, Jaumann et al., this special issue.), a hyperspectral microscopic imager (MICROMEGA, Bibring et al., this special issue), a magnetometer (MASMAG, Hercik et al., this special issue) and a radiometer (MARA, Grott et al., this special issue). The overall payload has a mass of ~3 kg. After landing in 2018/19 on the C-type asteroid, (162173) Ryugu, the four instruments will study in-situ its surface morphology and geological setting, its regolith structure, texture and composition, the thermal and magnetic properties of the surface on up to 3 landing sites, enabled by MASCOT's ability to hop across the asteroid (Jaumann et al. 2014).

The mission is fully complementary with the next asteroid sample return mission to be launched in September 2016, is NASA's OSIRIS-Rex to the B-type asteroid (101955) Bennu. Other sample return missions, similar to the proposed ESA Mission MarcoPolo R (Barucci et al., 2012) or possible future Comet Surface Sample Return missions would complement our understanding of the nature and the variability of the small bodies in the Solar System.

2 The Mission Overview and Operations at the Asteroid

The Hayabusa2 (HY2) spacecraft (s/c) with the MASCOT landing package (lander) onboard has lifted up from Tanegashima Space Center on Dec 3rd, 2014. After an Earth Swing by at the End of 2015, the spacecraft will go into direct cruise towards the asteroid. The interplanetary cruise will take approximately 4 years, with MASCOT nominally off except for commissioning and periodic monitoring and calibration activities. The arrival of HY2 at NEA (162173) Ryugu is expected to be in 2018 following by a ~1.5 years of survey and near asteroid operation phase (including deployment of the Minerva and MASCOT rovers/lander and in situ investigation, impact & sampling). Hayabusa2 will depart in December 2019 and return to Earth in December 2020. The mission outline is captured in Figure 1

Figure 1: Hayabusa2 Mission Baseline.

After a global mapping phase in order to characterize the asteroid surface and to determine the anticipated landing site based on its scientific relevance and under landing safety constrains MASCOT will be released towards the surface, either

during a dedicated descent or during one of the sampling touchdown rehearsals. Note that Hayabusa2 will not be orbiting around the asteroid, but rather hovering in an axis fixed in inertial space (joining the asteroid and the Earth). This fact narrows down the range of latitudes over the surface at which MASCOT can be deployed. This maneuver foresees HY2 to descend to a separation altitude of at less than 100 m over the surface, at which point MASCOT will get ejected via a spring mechanism that will provide a delta V of approximately 5 cm /s. The lander will fall onto the asteroid surface under the effects of its weak gravity field (see Table 1), followed by a bouncing period of unknown duration, and depending on the surface characteristics strengths before it comes to rest in an unknown orientation. The descent to the asteroid after ejection will take approximately 20 – 30 min, with communications to Hayabusa2 maintained throughout that period. If possible, MASCOT will also take camera images of the asteroid during descent.

Table 1: Parameters of NEA (162173) Ryugu (formally denominated as 1999JU3).

Parameters	
Mean volume-equivalent diameter (km)	0.87±0.03
Bulk density (kg/m^3)	1300
Spin period (hrs)	7.63±0.01
Spin axis (J2000), positive pole	λ_ecl = 73.1° β_ecl=-62.3° retrograde rotation Obliquity=151.6°
V_{esc} (m/s)	0.37±0.03
Thermal inertia (global average) (Jm^{-2} s$^{-0.5}$ K^{-1})	Notional: 400
Emissivity	0.9 (assumed)
g (m/s^2)	
Surface fraction covered with craters	0.4 – 0.9

After MASCOT's deployment, Hayabusa2 will return to its home position 20 km above the asteroid surface whereas a location of MASCOT's final rest position on the surface will be performed during this phase with the navigation camera if possible of HY2.

In order to conduct scientific operations, MASCOT must orientate itself and perform an selfrighting action in case it is not oriented in its nominal attitude with the bottom plate on the surface (see Fig. 2).

After completion of science operations at the first location, which will approximately take 1 asteroid day (equal to approximately ~7.6 hours), MASCOT

can be relocated to another site. The same internal mechanism which will be used for the self-righting will then be activated to send MASCOT in an uncontrolled hop across the surface at a distance of up to 220 m. Further scientific activities will take place, and then, power depending, a second hop may be possible, followed by self-righting if necessary.

Figure 2: The 'on-asteroid' surface operation baseline of the MASCOT lander

The first order scientific objectives for MASCOT is to investigate at least at one position: (1) the geological context of the surface by descent imaging and far field imaging in-situ; (2) the global magnetization by magnetic field measurements during descent and any local magnetization at the landing positions; (3) the mineralogical composition and physical properties of the surface and near-surface material including minerals, organics and detection of possible, near–surface ices; (4) the surface thermal environment by measuring the asteroid's surface temperature over the entire expected temperature range for a full day-night cycle; (5) the regolith thermophysical properties by determining the surface emissivity and surface thermal inertia; (6) the local morphology and in-situ structure and texture of the regolith including the rock size distribution and small-scale particle size distribution; (7) the context of the observations performed by the instruments onboard the main spacecraft and the in situ measurements performed by MASCOT ('cooperative observations') and provide documentation and context for the samples and correlate the local context of the in situ analysis into the remotely sensed global context; (8) the body constitution on local and/or global scales and to constrain surface and possibly sub-surface physical properties; (9) the context of the sample collected and returned by the main spacecraft by qualifying its generic value and processed/pristine state and thus support the laboratory analysis by indicating potential alteration during cruise, atmospheric entry and impact phases.

3 The MASCOT Lander and its Payload

3.1 System Overview

The MASCOT surface science packet (so called "lander") has a total volume of about 0.3 x 0.3 x 0.2 m^3 and a total mass of ~ 9.8 kg. In addition to the four scientific instruments (MASCAM, MicrOmega, MARA and MASMAG) it accommodates

all support elements (i.e. data handling, power, communication, attitude determination, and passive thermal control) for the on-asteroid operation.
The lander structure is made of a lightweight carbon fibre framework to support the passive thermal control elements (Single Layer Insulator=SLI) and the antennae for communication during surface operation. The lander is equipped with a mobility mechanism and a suite of attitude determination sensors to self-right itself into correct instrument orientation and to perform relocation via hopping on the asteroid's surface. Control, housekeeping, autonomy, data handling and local processing power are provided by a redundant on-board computer (OBC). Power is supplied by primary batteries via a redundant power distribution unit (PCDU).

Figure 3: MASCOT Lander Module.

The lander's configuration is divided into two segments: a warm compartment containing the electronics box with the majority of the electronics, the battery package and the mobility mechanism, and a cold compartment housing the scientific instruments. The four lateral external walls are covered with aluminum vaporized kapton (SLI), with the top surface being used as the main radiator.
The design goal was to operate up to two asteroid days on the surface. Communication is established via relay by the Hayabusa2 s/c (the so-called mothership). Due to the short duration of surface operations, the amount of direct telemetry to and control commands from Earth is extremely limited, requiring almost complete autonomy of the lander. Each subsystem will be described in the later sections in detail.

3.1.1 Autonomy

The on-surface operational concept of MASCOT poses some interesting challenges. These are on the one hand attributed to uncertainties in the actual properties of the asteroid, which can only be resolved during the global characterization of the same, shortly before MASCOT separation from the mother spacecraft. On the other hand, given the long signal round-trip time and bearing in mind the constraints regarding the real-time downlink of data from HY2 to the ground; the on-surface operational phase has to be done completely autonomously, i.e. without ground intervention.

For these reasons, we have implemented a decision making engine in the software of the on-board computer (OBSW), the MASCOT Autonomy Manager (MAM). In its baseline design the MAM is programmed as a nominal state machine with internal state and transition logic.

This approach has been identified as a compromise between simple pre-programmed timeline execution and a much more complex kind of intelligent onboard mission planner and optimizer. Core decision nodes and state transitions for the MAM are:

(i) decide if an attitude correction is necessary after touchdown or after a hopping manoeuvre, factoring in the GNC sensor information and other available data,

(ii) activate the scientific instruments according their pre-defined (nominal) sequence,

(iii) decide if MASCOT is ready to execute a hopping manoeuvre to a different site on the asteroids surface

(iv) adjust the course of action depending on system resources and states (energy monitoring and management as well as failure management).

All of these decisions involve a high level of system "knowledge" or awareness of the system itself. Also, the number of possible states is still very high, thus careful system level verification and validation is/was required.

3.1.2 Interface between MASCOT and Hayabusa2

During cruise and until release, the MASCOT lander is carried in a mechanical and electrical support structure (MESS) attached to the HY2 spacecraft on its –Y panel. During this time MASCOT is mostly inactive; thermal control and power supply for in-cruise operations are provided by the Hayabusa2 mothership.

Table 2: Mass budget of the MASCOT Lander Module and the MESS.

MASCOT Lander	Mass [kg]
Mobility	0,52
GNC	0,26
OBC	0,49
Communication	0,52
Power (Batteries and PCDU)	1,82
Structure (incl. Ebox)	2,13

Thermal	0,41
Harness	0,55
Payload	
MicrOmega	2,1
MAG	0,24
MARA	0,26
MASCAM	0,46
MASCOT MESS (incl. umbilical and harness, separation mechanism, MLI, RF Antenna, calibration target for MARA and MASCAM)	1,23
Total	**11,02**

The MESS will remain attached to Hayabusa2 after the lander has been ejected. The MASCOT and MESS accommodation within the Hayabusa2 spacecraft is shown in Figure 4.

Figure 4: MASCOT and MESS (left). MASCOT attached on the –Y panel of the HY2 spacecraft (right).

The MASCOT lander is electrically connected with Hayabusa2 via an umbilical that runs from Hayabusa2 through the MESS to MASCOT, see Figure 4 (left). The umbilical connector which connects MESS and MASCOT across the separation plane is based on a MIL standard Matrix KJ connector with gold-plated spring-loaded pins and concave platinum counter faces on the opposing sides. Even though the design has heritage from Rosetta Philae the umbilical connector has undergone an extensive qualification program including environmental and functional unit level tests to assure proper functionality of this mission critical component.

3.2 The lightweight CFRP Structure and the common Electronic Box

As previously mentioned the MASCOT structure (Lange et al., 2012 & Lange et al., 2014) consists of two main elements: The Lander Module (LM) itself to be ejected from the mothership and operated on the asteroid surface, and MESS, the interface structure supporting the MASCOT LM on the mothership. The structure of MASCOT is mainly driven by the required stiffness, with a minimal first system Eigenfrequency of 120Hz. Additionally, the strict mass requirement and the available stowed volume make the design even more challenging. Overall the LM's rectangular package measures 0.275 x 0.290 x 0.195 m³. This volume again is split

by a central wall into two segments, a warm bus compartment containing the majority of the electronics in a dedicated common electronics box (E-Box) and a cold science compartment containing the payloads (see Figure 3). The E-Box is made from 6 separate aluminium plates providing thermal and radiation protection to all included PCBs. Further it serves as the structural interface for the Battery Package, the Communication Transceivers ('Child COM') and the Mobility Mechanism. The segmented E-Box' design uses, to save mass a combined approach of framework elements and shear walls, resulting in a total mass of less than 750g. A thermal-conductive insulation from the main structure is realised by the use of PEEK (polyetheretherketone) washers and dedicated titanium feet.

3.2.1 Lander Module Structure

In order to meet the mass requirement the MASCOT LM is built from an ultra-lightweight CFRP (Carbon-Fiber-Reinforced Plastic)-foam sandwich framework structure. Most of its struts consist of a 0.125 mm load-carrying carbon fibre-reinforced plastic face sheet and a 5 mm foam core. In total, the highly integrated lander structure has four external side walls, one internal vertical/middle wall, the base plate and a top plate. The top plate aluminium sandwich serves next to its structural function as radiator, too. To allow late-access activities, such as the installation of the battery or making safe-arm connections, the radiator has been divided into the fixed main radiator and a hatch-like removable sub-radiator.

In order to hold the MASCOT LM during launch and cruise, a non-explosive actuator (NEA), see section 3.6 on '*Separation'* is included on the MASCOT LM-sided part of the separation mechanism, which is mounted to the middle wall. A rod connected at one end to the MESS and at the other to the NEA provides a clamping force of 2.5 kN introduced into the middle wall. Hence the four bearing points of MASCOT LM are pulled into their MESS-sided counterparts, thus ensuring a firm connection between the MASCOT LM and the MESS.

Beyond its inherent structural functions, the framework structure supports functional surfaces for thermal control, attitude control sensors and radio link. For the radio link the antennae are connected to the sub-radiator and a galvanic copper-plated CFRP (carbon fibre-reinforced plastic) plate on the MASCOT LM's bottom plate (see Figure 6).

Figure 5: MASCOT Lander Module structure STM2.2 (bottom up).

3.2.2 MESS – Mechanical Electrical Support System Structure

The Mechanical Electrical Support System (MESS, see Figure 7) was designed to provide the required interface functionalities to Hayabusa2. To guarantee MASCOT's required inclined (15°) and recessed position within the HY2 -Y-Panel for the MESS structure the same framework design principle as for the MASCOT LM is applied. However, unlike the separate CFRP-foam sandwich walls, the MESS has 3 mm thick solid CFRP struts. These are again interconnected with L-shaped CFRP shear straps between each other. At its lower side MESS is fixed with 6 feet to the -Y-Panel. From there the load path is through the framework struts to the LM's four counterpart bearings in the MESS cavity's corners (see "MESS bearing corners", Figure 8, left).

In order to decouple Hayabusa2 thermally from the MASCOT LM during cruise and to provide thermal insulation after MASCOT's deployment, the entire volume created by the struts and occupied during cruise by MASCOT is surrounded by Multilayer Insulation (MLI). Between the MESS feet and the Hayabusa2 –Y-Panel fibre-reinforced PEEK insulators are used (see Figure 8, right).

Figure 6: MASCOT Lander Module FM structure inside of the MESS FM structure.

Figure 7: MESS STM structure with location of details in following figure.

Figure 8: Details of MESS FM bearing corner (left) and MESS FM feet insulator made of fiber-reinforced PEEK (right).

3.3 The Thermal Design

The Thermal Control System (TCS) of the MASCOT lander has to satisfy the diverse requirements of all mission phases. For cruise phase and near asteroid operation these requirements include keeping the battery pack at a low temperature of -30 °C with varying HY2 boundary temperature between -30 to +60 °C; limiting heat exchange between MASCOT and the spacecraft to ± 5 W, due to restricted spacecraft power delivery to Mascot. During periodic commissioning activities the TCS has to ensure operational temperatures for the electronics (at least -35 °C) and payloads for the execution of health checks and scientific equipment calibration. TCS operation at 'asteroid approach' during the HY2 descent phase includes the thermal impact of asteroid IR thermal radiation, and during the 'hot' and 'cold'

on-asteroid phases the effect of the day–night cycle asteroid surface temperature change, sun light (solar constant: 1370 W/m2) and asteroid surface albedo.. To withstand these thermal challenges, MASCOT TCS is designed to be semi-active during its 4 years of cruise and near asteroid operation, based on the delicate thermal interaction between heaters powered by the main S/C, heat pipes, coatings and insulation elements. On the other hand, on the asteroid, MASCOT has to dissipate the heat produced internally by the electronics and payloads in the most efficient way and be protected from external heat fluxes.

In order that the lander can survive the cold cruise phases and the hot on-surface phase (i.e. maximal heat dissipation) two solutions have been implemented:

a) Variable conductance heat transfer technology to dissipate the heat from the electronic box (the most dissipative element) to the radiator (Figure 9).
b) The available heating power on the most critical parts (electronic box, battery pack and MicrOMEGA payload via a fully redundant power line from HY2) is point distributed

The lander thermal design has a mainly passive approach, focusing on coatings selection, interfaces tuning and insulation. MLI blankets are used where space is available: to partially insulate the electronic box from the rest of the lander.

Figure 9: Structure of MASCOT thermal control system (left); heating power distribution and heaters lines (right). All controlling lines are redundant. MESS structure, MESS MLI will be the part of HY2 spacecraft after MASCOT separation

After a trade-off phase during which the possible alternatives in terms of variable heat transfer capabilities were studied, the technology adopted was a heat pipe solution which has all the visible outer attributes of constant conductance heat pipes but the thermal performance was similar to the ones of variable conductance heat pipes. They were developed and built by the National Technical University of Ukraine “Kyiv Polytechnic Institute”, and already had limited heritage on the SKALA (1980), Fragment (1983), and Magion-4&5 (1995, 1996) missions. Two 3-D heat pipe shell configurations with an external diameter of 6 mm and a total length of approx. 0.48 m with 4 bends were required for thermal connection of the electronic box with the main radiator through MASCOT’s tightly occupied inner space. The heat pipes underwent qualification and acceptance tests, including thermal characterization tests of the HY2 temperature range from -76 to +60 ºC,

conducted with two geometries. These have shown the desired thermal performance (Figure 10). The heat pipes' thermal resistance is defined as follows:

$$RHP = \frac{T_{inp,av} - T_{out,av}}{Q_{trans}}$$

where $T_{inp, av}$, $T_{out, av}$ are the average temperatures of the heat input and output zones of heat pipe. The transferred heat power, $Q_{trans,}$ has variable character and autonomously changes its value of nearly two orders of magnitude as a function of heat sink temperature, T_{sink} and the transferred heat power Q_{trans} (see Figure 10).

Figure 10: Heat pipes performance: thermal resistance as the function of heat sink temperature with stratification on transferred power (a) and transferred power with stratification on heat sink temperature (b). I, II – approximate areas of operation in cruise and on asteroid surface correspondently

While keeping at a minimum the heat losses to the exterior during cruise; the lander is switched ON in the proximity of the asteroid instead and will start dissipating heat. Thus the heat pipes increase their thermal conductivity, limiting the temperature increase inside MASCOT, particularly when it is still together with HY2. When released, the colder external conditions will provide additional heat balance.

The scientific mission is constrained by the lifetime of the battery and the temperature behaviour of the subsystems and payloads, depending on the internal dissipations and the external environmental conditions. The cold cruise phases (when the heating system is set to keep the battery pack above -40°C) are necessary to maintain the initial charge of the battery (i.e. assuring long lifetime on the surface of the asteroid). On the asteroid's surface the dissipations inside MASCOT and the external conditions become most relevant. Both these aspects have been investigated. In close collaboration with the power subsystem, the dissipations inside the lander were modelled taking into account the planned operations for both the free fall case and the on-asteroid scenarios. The external conditions were modelled in particular for the surface temperature profiles, based on the landing date and evaluated via a thermal model of the asteroid's surface, assuming different plausible values for the thermal inertia. These analysis resulted in multiple cold/hot worst case scenarios for the lander on the surface (Figure 11) impacting its ability to reject heat and its internal thermal behaviour.

Figure 11: Possible MASCOT landing locations on the asteroid surface. The asteroid models [RD…] have been used for prediction. Averaged per asteroid day temperature pattern is shown

Similar conditions and scenarios were also tested through extensive thermal vacuum campaigns. In every test, the temperature values measured on MASCOT and MESS never violated the respective limits and the results were used in order to tune the internal interfaces of the system for thermal model correlation purposes and improvement of the model itself.

3.4 The Avionics and Communication

3.4.1 On-board Data Handling System

The on-board computer (OBC) is designed to be dual redundant and consists of four boards, which are accommodated in the MASCOT electronics-box. The 4 boards are less than 500gr and require 2.65Watt on average, and 4Watt peak power in total. Two cold redundant CPU-boards are cross-trapped by internal Spacewire data links with two hot redundant I/O boards. The OBC interfaces to all MASCOT subsystems and payloads via point to point serial data links (RS422 UARTs and Spacewire) and dedicated, discrete analog/digital I/O interfaces.

The OBC software (SW) implements the Mission Autonomy Manager (MAM, see section 3.1.1‘Autonomy’), the Failure Detection Isolation and Recovery (FDIR) function, the acquisition and compression of the housekeeping and scientific data and their storage, retrieval and subsequent transmission to HY2 orbiter via the Communication subsystem, when the radio-frequency link is available.

The I/O boards are each equipped with a NAND FLASH memory device, handled as a dual hot redundant mass memory by the SW mass memory, effectively achieving over 450 Mbytes data storage, error protected by a Reed Solomon encoder/decoder.

The cold redundant CPU as well as the hot redundant I/O-boards are operated in a worker-monitor redundancy concept, whereby the functionality of the “worker” is supervised by the “monitor”. The monitoring and CPU switch-over logic is residing in the FPGA of each I/O-board, independent from the SW.

The following diagram shows the internal architecture of the OBC and its interfaces:

Figure 12: MASCOT OBC Schematics

3.4.2 Communication

The main principle of the communication between the MASCOT lander and the HY2 mother spacecraft is a shared system with the three Minerva Rovers also on-board (Tsuda et al., 2013), that are also part of the HY2 mission. The MASCOT lander is equipped with redundant Child-COM (CCOM) transceivers which were provided by JAXA to communicate with the Parent-COM (PCOM) transceiver on HY2 side together with JAXA's three rovers based on a half-duplex communication and time division multiple access (TDMA) methods. Communication during the 3-4 years of cruise is performed via a dedicated antenna attached to the MESS and connected to the HY2 s/c. Afterwards, starting from the separation of the lander from the mother spacecraft, communication is established by two patch antennas (one on the top surface and one on the bottom which ensuring quasi-omnidirectional coverage). All three antennas as well as the corresponding RF-cables and couplers were provided by CNES.

An overview on the communication chains is described in Figure 13.

Figure 13: RF communication chains between MASCOT and HY2

The system harness, connected to the MESS antenna, allows nominal communications for command and telemetry links between the MASCOT lander (embedded in the MESS) and HY2 during the cruise phase, and possibly for a few minutes after the lander's separation.

The mission harness, connected to the OME-A antenna, will be used for command and telemetry links during the descent and on-asteroid mission phases. The OME-A antenna provides sufficient radiated power to allow a nominal communication with MASCOT from few hundred meters up to 20-kilometers above the asteroid's surface, the Home Position of HY2 during the MASCOT mission.

Each transceiver (CCOM on MASCOT, PCOM on HY2) can be operated with two radiated power modes: a low-power mode (P(RF) = -15 dBm) and a high-power mode (P(RF) = +20 dBm for CCOM / P(RF) = +30 dBm for PCOM). These power modes can be dynamically triggered during each mission phase depending on the link budget requirements (e.g. the low power mode is preferably used during the cruise phase as the coupling antenna factor between MESS and MASCOT antennas is high enough). The CCOM transceiver used on-board MASCOT is depicted in Figure 14 with several associated features.

Figure 14: CCOM transceiver overview

- Size: 80 x 50 x 15 mm^3
- Mass: < 100 g
- Electrical power consumption: 1.7 W (both receiving and transmitting)
- Radiated power levels: -15 dBm (low-power mode) / +20 dBm (high-power mode),
- TX Frequencies: 954 MHz (Channel 2) / 958.5 MHz (Channel 1)
- RX Frequency: 954 MHz (Channel 2)
- Effective TX data rate: 37.037 kbps @ BER: 10^-5,
- Effective RX data rate: 1.736 kbps @ BER: 10^-6,
- Modulation: BPSK (both TX and RX)

In terms of mission analysis, several studies are being performed taking into account different asteroid soil compositions and corresponding simulated effects on the radiation pattern of MASCOT antennas in order to check the link budget performance and subsequently the achievable communication range between HY2 and MASCOT. These studies will help to define the final altitude of HY2 above the asteroid's surface for the mission phase.

The omnidirectional coverage of MASCOT is ensured by using two circular polarized patch antennas working around 958.5MHz. Considering the very small space available to accommodate the antennas and the frequency band, a high permittivity substrate has been used to reduce the antenna's sizes. The two MASCOT antennas ensure -10dBi of gain in each hemisphere on MASCOT structure.

Figure 15 : MASCOT antennas

Moreover, for the cruise phase, a Planar Inverted F Antenna (PIFA) on high permittivity substrate was used to reduce drastically the antenna size.

Figure 16 : MESS Antenna

All antenna's designs have been optimized to the MASCOT and MESS structure using Electromagnetic software (FEKO) taking into account material characteristics, and the overall antenna models were measured on a MASCOT and

MESS mock up in the Compact Antenna Test Range (CATR) of CNES in Toulouse to verify the radio electric performances.
Finally, the antenna was tested in thermal vacuum from-120°C to +120°C to validate the RF performances stability in a wide temperature range.

Figure 17 : MASCOT antennas optimized on structure by EM simulation

Figure 18 : MASCOT Antenna Flight Model

Each MASCOT antenna is linked to the CCOM receiver with a harness composed of RF cables and couplers working in the dedicated UHF frequency band.

Figure 19 : MASCOT Harness

3.4.3 Power

MASCOT can operate from two power sources: via the umbilical connection from Hayabusa2 for commissioning, during in-flight check-outs and maintenance activities, in the same manner as electrical heater control during interplanetary cruise. Once MASCOT is separated, power is supplied by the internal non-rechargeable battery for descent and asteroid surface operations.

3.4.3.1 The Hayabusa2 Umbilical Supply

Power is provided from a single switched output of the Hayabusa2 power subsystem via a fully redundant connection to MASCOT. The power interface is capable of supplying up to 50 W to the lander. HY2 uses a nominal bus voltage of 50 V that is directly switched to MASCOT as well as other instruments and bus units. When its power line is turned 'ON', MASCOT automatically activates to a boot configuration that activates the OBC for command reception and processing and – after a time-out for detection of an EGSE connection at a physical electrical interface – activates the RF communication link. This initial configuration is also the minimum power configuration with command chain redundancy enabled. Under certain off-nominal conditions, at the occurrence of which MASCOT should nominally be turned off, the HAYABUSA2 bus voltage could drop to about 30-35 V. MASCOT is nevertheless designed to be fully capable of operation also on this level to enable controlled shutdown.

3.4.3.2 The MASCOT Battery

After separation from the mothership, power is provided by a battery consisting of nine SAFT LSH20 D-size non-rechargeable Li-$SOCl_2$ primary cells (Spotnik et al., 2006, Eisenmann, 1996, Evans et al., 1989 and Cho, 1987) The cell type used has flight heritage; in fact, due to timely availability the cells used in the development of the MASCOT lander are from exactly the same batch as those used on the PHILAE cometary lander. While they powered the landing and first activity period of PHILAE on comet 67P/Churyumov-Gerasimenko as part of the ROSETTA mission, they also provided precious reference data for future lifetime estimates in the operations planning of the MASCOT lander.

The available mass and volume for the design of the battery was given by the overall system constraints, the suite of science instruments and respective operations concepts, and the spacecraft bus required to support these. The battery simply filled up all remaining volume and mass at cell-level increments: at 9 cells possible by volume the optimal configuration was a 3s3p topology (see Figure 20). The string length, by coincidence of available volume and mass, corresponds to the minimum required number of cells in series to achieve a bus voltage within the limits of the concurrently evolving PCDU design. A 4s2p topology also possible within the same constraints would have provided a higher bus voltage but would also deliver significantly less useable energy and offer less redundancy.

Figure 20: FM Battery of the MSC lander, top side (left) and bottom side (right).

On the timescales of MASCOT, the battery was a long-lead item. To provide flexibility during the Engineering and AIV process of the project, all strings and other electrical elements in the battery are mutually isolated. The definite configuring connections can therefore be made externally which enabled battery design and production to proceed with minimum interdependence while the system-level power management design and the Hayabusa2 interface still evolved in parallel. Each string has a dual Schottky blocking diode to protect against charging current flow during Hayabusa2-powered operations, and a polyfuse device ensuring self-resetting protection against high short-circuit or overload-generated discharging currents at string level without incapacitating the whole battery at once.

The battery enables asteroid surface mission operations on 2 asteroid days, with the actual lifetime being highly dependent on the on-surface sequence and timeline of

science operations as well as the thermal environment. The nominal capacity of the battery is 255 Wh at the relatively high cell load imposed by MASCOT's intense science operations and related activities of the thus required bus infrastructure. In terms of specific performance parameters, e.g. Wh/kg or Wh/m³ at unit level, this is still somewhat above the capacity that could have been achieved with PHILAE-era rechargeable cells under the same general constraints and conditions. As recently demonstrated by the adventures of PHILAE the unknowns of potentially rugged terrain near the first landing site can introduce unexpected factors in spacecraft operations. The intended concept of MASCOT relocation involving an initial leap and a series of bounces, like the unintentional bounces of PHILAE, is best described by an initial energy and impact dissipation constrained random walk. With this in mind, the MASCOT team opted for an albeit only moderately higher assured energy capacity without the capability to test actual capacity available before separation or to recharge, as provided by the primary cells chosen. The option of a pre-separation testable but initially somewhat lower pre-charged energy capacity with photovoltaic re-charging and/or extension depending on the uncertainties of locations and terrain as provided by secondary cells was consequently discarded.

The most important consequence following from the choice of primary cells is that self-discharge and leakage discharge has to be rigorously minimized by careful electronics design and manufacturing and very cold storage under rigid thermal control. Also, since the performance of primary cells with low self-discharge is more dependent on temperature and discharge current, much more effort has to be invested in operations planning and system-level optimization towards warm battery operational condition. Finally, there is no go-around to try again: primary cells give only one chance.

3.4.3.3 MASCOT Power Conditioning and Distribution Unit

The Power Conditioning and Distribution Unit (PCDU) manages power-up activation of the command chain subsystems during cruise check-outs and during the separation process. It converts power from the relatively high-voltage 50 V power bus of the mothership to the battery unregulated power bus (UPB) of MASCOT. While powered by Hayabusa2, the UPB is supplied by an isolated and regulated voltage just above battery strings' open-circuit voltage of about 11 V. This ensures that the battery cannot accidentally discharge into the UPB while MASCOT is powered and the battery switch could turn 'ON' unintentionally.

Potentially dangerous charging leakage is minimized by the string reverse protection diodes in the battery, the battery switch design in the PCDU, and the small voltage difference. Due to this feature, it is also easily possible to alternate between battery power and Hayabusa2 power during the final checkout of MASCOT immediately prior to separation by simply removing and re-applying external power after turning the battery 'ON'. A brief loading of the battery before separation verifies that it has been switched on and is healthy. A brief power draw is also necessary to overcome the voltage delay phenomenon characteristically of Li-$SOCl_2$ chemistries (Eisenmann, 1996 & Spotniz et al., 2006) by a controlled depassivation while a fall-back power source is still available in case the UPB voltage drops so low as to cause a system restart.

3.4.3.4 PCDU Architecture

The PCDU provides switched outlets of direct unregulated non-isolated battery bus (UPB) voltage as well as several non-isolated and isolated regulated voltages which are further distributed to the power consumers by downstream switches. Key activation and command chain related supply functions and load safety as well as command control circuits are redundant while certain exclusively science payload related functions are single-string implementations. However, when seen from the system level some semi-redundant functionality is added for robustness where feasible. All power switching in MASCOT is done by MOSFET switches; there are no electromechanical switches carrying electrical power. This approach enabled accommodation of a reasonably robust power subsystem within the tight system constraints. The PCDU consists of two card modules plugging into the system Backplane within the E-Box structure that provides common shielding, mechanical support and card mounting guide rails which also serve as the main thermal conductive path. Each PCDU module consists of a flip-over pair of rigid multilayer PCBs cards with an integrated flex layer segment serving as interconnection. Redundancy management signals are shared between both cards via the Backplane that connects all cards in the E-Box.

Figure 21: MASCOT PCDU architecture (top).

The battery is mounted directly on top of the E-Box, creating a thermal path between the cruise heaters inside the battery and the electronic components as described in section 3.3.

Figure 22: MASCOT E-Box Backplane & Cards.

The MASCOT PCDU is controlled redundantly by an FPGA on each PCDU module supporting cross-connected control lines to the power converters and switches on both modules. Each FPGA is connected by a point-to-point serial interface to both redundant sections of the OBC. Timely actuation of the PCDU is assured by multiple transmission of the commands from the OBC which are sent once on each of the four available connections between both units. Telemetry consisting of all status flags and measurements of currents, voltages and temperatures in the PCDU is collected and formatted by their redundant FPGAs into a packaged set. It is sent to the OBC via the same four serial interfaces. The rate of these telemetry transmissions to the OBC can be commanded. The maximum rate is 2.5 of such packaged sets of telemetry per second.

3.4.3.5 PCDU Operation and Integration with the System and a Non-Rechargeable Battery

The battery needs to be well isolated against unintentional discharging during the 4-year interplanetary cruise by the PCDUs‘redundant power activation circuits which also have to maintain isolation against unintentional charging during cruise check-outs by power then applied to the bus of MASCOT via its PCDU from the mothership. For this purpose, two parallel redundant, triple in series MOSFET switches are used, one on each PCDU module. Beyond the nominal telecommand path, the respective half-section of the battery switch can also be controlled by an external discrete input line to either PCDU module by a Mechanical Separation Detection (MSD) circuit that detects an unambiguous signal of the ejection of MASCOT out of its support structure, MESS. This MSD circuit then closes a battery-supplied, normally-open signal path that forces both battery switches ‘ON’ permanently to ensure MASCOT is and stays activated after separation. In case the command link between both spacecraft cannot be sufficiently established to first turn the battery ‘ON’ before separation, MASCOT can simply be separated as a last resort and will turn ‘ON’ forced by activation of the MSD circuit, though without

controlled depassivation of the battery, as a simple one-step fall-back to the whole nominal activation path involving RF link, OBC and PCDU.

3.4.3.6 Safe Activation of MASCOT

There are several breakwire connections are in the zero-force separation connector between MASCOT and MESS for separation detection by Hayabusa2 and the then nominally already activated MASCOT OBC, respectively, but this method cannot be employed on MASCOT for activation itself since breakwires for this purpose require, however little, constant power from the side which reads the signal. For an order of magnitude example, one typical power transistor leakage rate of 1 µA over the assembled spacecraft lifetime consumes about ½ Wh of energy or up to 5 minutes of surface lifetime at minimum power. Thus, a zero-power method has to be used in the MSD network for separation detection. The MSD interface in the PCDU was defined and fixed relatively early in the project such that the actual MSD detection principle, signal processing method, redundancy concept, and detailed circuit design could evolve concurrently and independently from that of the PCDU. In the end, due to separation mechanical interference considerations and volume constraints, actual separation switches at the mechanical interface were considered risky and/or infeasible and thus discarded in favour of a very compact 4-fold redundant detection circuit using polarized magnetically self-latching relays to redundantly drive a simulated 2s2p topology MSD switch network at the MSD interface of the PCDU. This Safe Activation Relay (SAR) circuit evaluates electrical separation command signals to MASCOT at the umbilical separation connector by analogue-electromechanical signal processing means. The SAR contains the only electromechanical active components on MASCOT. Although difficult to obtain, components with very extensive flight heritage were selected. The actual circuit design was adaptable to the component version which was available off the shelf within the schedules required by the MASCOT project timelines. The SAR circuit was implemented only for the FM and FS of MASCOT. The SAR EM and EQM circuit testing was performed in parallel to MASCOT FM integration, largely after delivery of the FM SAR units, also because the key component quantity available was only sufficient for 3¾ SAR units being in parallel use, requiring some shuffling of parts between EM, EQM and designated FS unit. Thus, also the SAR circuit implementation and accommodation in MASCOT was such that several signal processing and output configurations could have been set

by late change access at the SAR already in the FM integration campaign, effectively creating a general-purpose module with high re-use potential over a wide range of input signal and output interface conditions and configurations.

3.5 The On surface Mobility and GNC

3.5.1 Mobility

Since the MASCOT lander has no attitude control during its free-fall onto the asteroid surface guaranteeing that it lands on the baseplate and for the three science instruments (i.e. MicrOMEGA, MASCAM and MARA) to operate, the lander is equipped with "mobility" system to self-right MASCOT to its nominal orientation. The mobility consists of mechanics, electronics and an offline generator for optimized trajectories. The concept uses a small brushless DC motor with only 25 mm diameter to accelerate and decelerate an eccentric arm. The resulting reactive force applies jerk to MASCOT. Depending on movement parameters of the motor controller the eccentric arm generates jerk in different directions and enables MASCOT to hop or to self-right to its nominal position. Due to the mounting position of the mechanics (motor and eccentric arm) within the system, outside of the center of mass, a single degree of freedom in conjunction with the ground interaction can be used to flip and tilt in every direction. The trajectories are computed by multi-objective optimization on the ground. Before the lander is separated from the spacecraft the trajectory parameters will be uploaded from ground to the flight hardware for the last time. A precise offline multibody simulation model is used to predict the system behavior dependent on the specific asteroid parameters that will be estimated and improved during the approach of the spacecraft to the asteroid. Therefore the model covers:

- the dynamics and kinematics of the bodies of MASCOT, in particular the dynamics and kinematics of the mobility unit
- the contact dynamics including surface stick-slip friction between MASCOT and the asteroid surface modeled by PCM
- the current knowledge of the asteroid surface, gravity field and soil strength of (162173) Ryugu
- rigid or flexible modeling of MASCOT's outer CFRP-frame

Model verification and validation have been carried out using parabolic flight tests as well as high precision reaction force measurements in terrestrial laboratory environment.

Furthermore the model is used in order to determine suitable trajectories for both up righting and hopping. Therefore the model is wrapped in the framework TOMATO (Tool for Optimization of Mascot's Arm TrajectOry) based on MOPS (Multi-Objective Parameter Sythesis) (Joos et al., 2002). The framework utilizes several special step-wise optimization approaches in order to lower the computational effort and enable the use of genetic algorithms (Lichtenheldt and Schäfer, 2013).

The five tuners of the optimization are the characteristic parameters of the arm trajectory profile:

- acceleration and deceleration of the arm
- the arm's starting and end angle
- maximum rotational velocity of the mobility arm

For up righting, the objectives in the trajectory optimization are:

- binary: landing on the desired face
- minimization of the settling time of the system in order maximize scientific operation time
- minimization of the velocity normal to the surface and binary criterion to stay safely below the asteroid's escape velocity

For the hopping the same objectives apply, with the addition of the maximization of the jumping distance up to the first ground contact, as well as the final combined jumping and bouncing distance. Using this approach the simulated jumping distance to the first ground contact has already been increased by a factor of ~6 to the manually obtained trajectories (Lichtenheldt et al., 2015). Nevertheless, farther jumping also causes farther bouncing and longer settling times, as there is more energy stored in the system.

Figure 23: Jumping distance δ up to the first ground contact – path through 4 dimensional parameter space; coloring shows the arm end angle θ_a and marker size is correspondent to the initial arm angle θ_e (Lichtenheldt et al., 2015)

Figure 23 shows an example of the optimization path through the 4 dimensional parameter space for starting and stop angle of the mobility arm as well as its acceleration and deceleration. There by the flat area for higher decelerations shows

the potential to choose robust trajectories, which are especially important for up righting. In Figure 24the same plot is shown with different parameters on the plot axes. It clearly shows that the maximum jumping distance is dependent on the mobility arm angle.

Figure 24: Jumping distance δ up to the first ground contact – path through 4 dimensional parameter space; coloring shows the arm deceleration $a_{\mathrm{arm}}^{\mathrm{d}}$ and marker size is correspondent to arm acceleration $a_{\mathrm{arm}}^{\mathrm{a}}$ (Lichtenheldt et al., 2015)

For every possible six orientations of MASCOT there are three trajectories with different intensity levels stored in the autonomy manager MAM of the OBC. Once the lander is separated from the spacecraft it needs to initiate the self-righting and hopping autonomously to ensure proper behavior even when the communication link to the spacecraft is disturbed.

The mobility subsystem is essential for the success of the mission and was designed to be redundant if possible. Due to space and weight limitations the mechanics could not be realized redundantly but the electronics is implemented completely cold redundant. The OBC analyses the communication messages of mobility and decides when to switch to the other redundancy path. Communication with the OBC is realized via RS422. Figure 25 shows on the left the upper side of the flight model PCB. On that side the digital electronics with the FPGAs, the line drivers and the ADCs was realized. In Figure 26 on the right, there is the bottom side of the PCB with the analogue electronics shown. Located on that side are the motor controller, the radiation tolerant and ITAR free MOSFETs, the shunt resistors and the motor chokes. Since there are two redundancy paths that need to be coupled to a single motor, there is the need for a decoupling network. Considering the reliability and probability of failures an additional MOSFET was used to connect and disconnect the motor phases explicitly. This is the reason why there are nine MOSFETs for each redundancy path. To control a three phase motor, six power switches are used and additional three switches are needed for disconnecting the power electronics from the motor in case of malfunction. The separation of the nominal and redundant signal paths from the motor is essential to prevent unintentional short currents. The motor windings induce voltage when the rotor moves. This voltage needs to be considered and should not lead to a short that brakes the motor. Reliability can be improved only when the redundant signal path is completely separated from the motor.

Figure 25: Photo images of mobility flight model electronics PCB (on the left: top side, on the right: bottom side).

Figure 26 gives an overview of the mobility mechanics. A permanent synchronous motor with diameter 25 mm in combination with a harmonic drive HFUC8 gearbox deliver a repeatable maximum output torque of 3 Nm. The overall size of the cylindrical unit is Ø 31 mm x 64 mm. The eccentric arm is mounted to that, causing the necessary reactive force for moving MASCOT.

Figure 26: On the left: CAD sectional drawing of mobility unit (MobUnit) showing the compact fusion of Harmonic Drive gearing with brushless DC motor. On the right: CAD image of motor and eccentric arm.

The lubrication was chosen to prevent cold welding during the long cruise phase of four years. In that time the motor is moved during periodically conducted health checks only. The output shaft ball bearing consists of a combination of stainless steel rings, peek bearing cages and ceramic balls. This solution uses a non-metallic metallic combination which prevents cold welding. For the gearing bearing no hybrid ball-bearing are available in the appropriate size. Therefore MoS2 lubrication was applied there and also on the gear teeth. Finally a Dicronite DL-5 coating was used on the harmonic drive wave generator bearing. This may be not the best solution for continuously running application but still it is a good way considering the mission of MASCOT.

3.5.2 Attitude Determination/GNC

The motion state and the orientation on the asteroid surface of the MASCOT lander is determined mainly by two sensor systems to guarantee redundancy:
There are five optical proximity sensors (OPS), see Figure 27, mounted on five different sides of the lander. They consist of an infrared LED and an appropriate photo-diode. The light emitted by the LED is reflected by any object within the Field of View of the sensor. With this the asteroid's surface can be detected and thus the lander's ground facing side. To distinguish between reflected light from the LED and background illumination, e.g. from sunlight, the LED is on/off modulated and the signal from the photo-diode is correlated with this modulation.

Figure 27: Optical Proximity Sensor (OPS)

Six PCB-mounted photoelectric cells (PECs), see Figure 28, are mounted on each side of the lander to detect the solar direction. Due to Lambert's cosine law the output voltage is proportional to the cosine of the angle between sun vector and the normal vector of the cell.

Figure 28: A Photoelctric Cell Sensor (PEC) glued to MASCOT surface

This information is then passed through a histogram filter for multi sensor data fusion to determine which side of MASCOT is pointing to the surface. In addition, a decision logic is used to detect the motion status of MASCOT (Schlotterer et al., 2014).

To validate the function of the GNC subsystem, the behavior of the sensors has been identified at unit level. This information was then used to build mathematical sensor models. A dynamic simulator was designed including these sensor models together with the dynamics of MASCOT on an arbitrary terrain to simulate falling, bouncing and rolling of MASCOT. The simulator also includes the computation of the lighting conditions to stimulate the sensor models and all GNC related onboard algorithms. This gives us the possibility to test the behavior of the GNC system under different lighting and terrain conditions. An extensive simulation campaign was performed, varying initial conditions of the lander (e.g. velocity and attitude rate), sun elevation and terrain roughness.

In a second step, the GNC system was tested in the Software Design and Validation Facility (SDVF). This is a Hardware-in-the-Loop test facility with flight-like onboard computer (OBC) and I/O boards. The sensor signals are simulated using the same sensor simulation models as before.

In a last step, an End-to-end test of the complete GNC system has been done using the MASCOT flight-spare with real sensors and OBC and the final flight software. The asteroid surface has been simulated using a board with realistic optical properties and a spot-light as sun simulator. In this way the sensors have been

stimulated in a realistic manner while having the flight hard- and software with all its possible error-sources in the loop.

3.6 The Separation & On surface Operation

3.6.1 The Separation & Preload Release Mechanism

Once arrived at the asteroid, after HY2 has performed a global mapping and the landing site has been selected, MASCOT will be released to the surface, either during a dedicated descent or in the frame of one sampling dress rehearsal maneuvers. The mothership will descend to the separation altitude of 100 m at which point MASCOT will be ejected with a controlled low velocity in the order of a few cm/s. MASCOT will then fall to the asteroid surface without the aid of any attitude control under the pure influence of the weak gravitational field, before landing in an undefined orientation.

The separation process is a decisive factor for the outcome of the later mission. Several possibilities might impede the successful touchdown on the asteroid's surface and thus had to be taken into account for the design of such a deployable unit. For example, the lander module (LM) must not get stuck in its supporting frame (MESS), must not hit a part of the HY2 spacecraft and therefore has to have the correct trajectory after separation inside a small separation cone, and it must also not have an excessive speed leading to damage on touch down or bounce back to space. However, in order to meet again the tight volume and mass constraints, structural interfaces were minimized where the LM fixation to the MESS and its associated deployment functionality is based on four cup-cone shaped stand-off elements which are held in place by a single load-bearing bolt which will be released at separation. In this way, the LM walls and edges are decoupled from the MESS and no guide rails are required which are common such as for regular CubeSat dispenser pods. In this interface design, a minimal preload has to be maintained to ensure a secure contact in the cup-cone elements under all mechanical environments. In order to push the LM out of the MESS, a dedicated Separation Mechanism (SepM) was designed where the mechanism was constructed, again to reduce mass, as a simple single-shot device but featuring high reliability parts. This SepM consists of 4 main elements, namely the Pre-load Release Mechanism (PRM), a Non-Explosive Actuator (NEA), an Umbilical Separation Connector (UMC) and a miniaturized spring-loaded push plate (Push-off). The SepM operates

as a two-stage system. The first stage (Pre-load Release) is activated and controlled by MASCOT during one of the first cruise check-out activities soon after launch and the second stage (Eject Maneuver) is triggered by HY2 which initiates the terminal separation sequence while hovering above the asteroid.

Figure 29: Overview of separation mechanism

During Launch the MASCOT has to withstand the high loads and vibration. Thus the MASCOT LM is "locked" via a stored high preload of approx. 2500N to ensure that the LM stays embedded safely in the MESS not to damage HY2 or to get stuck at separation because of a distorted configuration. On the other hand a smooth separation requires the preload of the structure to be reduced to less than 200N before MASCOT's separation via activating the PRM to avoid a too high ejection speed, which could cause the LM to re-bounce from the surface and drift off into space.

The concept of the PRM comprises of two thermoplastic disks with heating foils stacked to a sandwich inside two opposing titanium pans see Figure 30. Two temperature sensors measure the heating process inside the device where both thermoplastic discs are made of polyacetal and will be mechanically weakened due to the increased temperature. This induced creeping process and consequently the movement of the pans towards each other will be driven by the initial pre-loading of the MASCOT structure, which is permanently under compression before activation. In order to keep a remaining load of approx. 200N for the cruise phase and the following separation process, four adjustable closing contacts will stop the motion and will detect electrically the successful preload release process.

Figure 30: Sketch of PRM CAD design (left) and FM model integrated in the structure (right).

Figure 31: The remaining preload force and PRM temperature during a melting process.

After activation of the PRM, the LM is still safely stored inside its frame. The remaining load transmission through the bolt, the PRM and the NEA is sufficient to sustain structural distortions which may arise due to temperature gradients throughout the remaining cruise phase. To initiate the terminal separation sequence, the NEA is triggered by a main-spacecraft command. The separation command is sent via the HY2 Igniter Box through a redundant trigger channel to the NEA's

redundant fuse wires. A fuse current of approximately 3A is needed on one of the channels and respected fuse wires for roughly 60ms to activate the release. The electrical interface for this command is the UMC which provides in addition a feedback signal to indicate MASCOT's separation upon disconnect. The connector design is based on a MIL standard Matrix KJ type body with spring-loaded pins (gold coated pogo-type pins) on one side and concave platinum counter faces on the other. The principle is based on PHILAE lander heritage and no extraction forces are needed for the separation of the connector bodies.

Figure 32: Sketch of Umbilical (left) and Flight Model (right).

When the actuator releases the LM from its position, the compression spring drives the push-off plate which pushes the LM into its eject trajectory. The energy stored in the compressed spring corresponds to MASCOT's required kinetic energy at ejection of v=0.05m/s (±0.01m/s). The Push-off plate consist of a CFRP-foam sandwich and at the interface to the separation bush the foam is replaced by an aluminium flange which provides a robust interconnection. The Push-off plate is shaped to fit on the struts of the LM and evenly distributes the pushing force. As long as the CoG of the LM resides within the effective area of the Push-off plate, the introduction of rotational moments is minimized. All elements of the SepM are designed according to ESA standards for the minimization of misalignment errors and cold welding risks and the total mass of the SepM is 277g, including PRM 85g, NEA 75g, UMC 65g and Push-off 52g, respectively. The functionality and performance of the SepM has been verified first by multi-body simulations and finally by extensive tests during dedicated microgravity campaigns using parabolic flights as well as drop tower experiments.

Figure 33: Push-off plate of separation.

As mentioned above, the SepM was designed as a simple, robust and very lightweight unit. While through its simplicity its reliability is increased, a drawback was found in the predefined and non-adjustable separation velocity as well as in a certain amount of uncertainties for the direction of the eject trajectory and the lander's rotational rate after clearing its support structure. However, through the combined verification of MB-simulations and microgravity tests it was possible to understand the systematic behavior of the lander during its separation process and

to trim the mechanism parameters accordingly. One of these key parameters is the separation velocity, which had to be within a narrow operational range in order to safely leave the main spacecraft and not to have an excessive speed upon surface touch down. Through the initial simulations it was found that the preload of the LM inside the MESS required to be locked at launch is elastically stored within the CFRP structure and would transfer to kinetic energy of the lander upon release. The main part of this load will be reduced with the PRM as described above. However, the remaining load of appr. 200N still adds to the energy given by the release. Also the UMC, which is a positive-force separation connector, introduces a non-negligible amount of positive energy as all of its 49 spring contacts work in parallel. Due to the compact volume of MASCOT it was necessary to place this connector a certain distance away from the lander's CoG. As a consequence, a rotational moment is introduced. To overcome all these side effects, the Push-off was adjusted to drive the lander using a short and relatively hard impulse rather than a long gentle push.

Figure 34: Separation velocity of the drop test campaign

The activation of the NEA opens the force closure and the stored energies of the structure, the UMC as well as the Push-off are released. Because of the major influence of the Push-off, the lander is pushed forward along the separation direction, but the secondary effects of the inherited tension of the structure and the UMC leads to the shaking of the LMin its xy-plane within the MESS. As shown in Figure 35, within the first 4cm of separation, roughly 40% of the initial energy given to the lander is dissipated due to these bounces off the frame walls. The apparent oscillation along the remaining separation distance is due to further but softer contacts with the MESS until the last contact determines the terminal eject trajectory. Although this last contact and consequently the last change in rotation cannot be predicted, the ongoing analysis of the drop tower experiments show that the lander stays within a small separation cone of ±5° and a slow tumbling rate between 0.5-1 rot/min.

Figure 35: The separation recorded by the ProGo.

3.6.2 On surface Operation

During the cruise phase, MASCOT will be switched on about twice a year for health check, calibration and maintenance activities. via the 50 V umbilical from HY2 and will communicate via RF-link to the MESS antenna on the HY2 spacecraft.

MASCOT will be released from HY2 into descent phase from an altitude of about 100 m above the asteroid surface. After MASCOT's separation, the HY2 spacecraft will ascent to an altitude of 20 km and act as the communication relay between MASCOT and the Earth.
The MASCOT lander will perform science measurements and calibration activities already during the descent. The magnetometer will perform one of its major science measurements during the MASCOT approach towards the asteroid surface. It is also planned to take several camera pictures from different distances to the asteroid. MARA (MASCOT RAdiometer) will perform measurements while looking into deep space as additional calibration of the instrument.
After first touchdown the lander will bounce until it comes to rest. The GNC sensors will determine the orientation of MASCOT relative to the surface. Then the lander will turn itself into its operational attitude., according to the measurements, with the baseplate towards the surface using the mobility mechanism for self-rigthening.
During surface operations MARA and MASMAG (MASCOT MAGnetometer) will measure continuously. The camera will take several pictures at different sun angles. During the asteroid night MicrOmega will perform its major scientific measurement, analyzing the grain composition. The camera measurements will determine the geological composition of the terrain, taking pictures with different illumination using colored diodes. MARA will measure the low temperatures on the night side of the Asteroid. Meanwhile the HY2 spacecraft will hover on the dayside of the asteroid. During the asteroid night MASCOT will have no communication link to the main spacecraft. The data will be uploaded during the following day.

After a full measurement cycle of all the instruments at the first landing site, the lander will relocate itself. Using the mobility mechanism it can hop up to 80 m across the asteroid surface. After hopping, bouncing and self-rigthening the lander will start its day/night measurement on the second landing site. MASCOT

operations will end after depleting its primary battery, which is designed for an operational lifetime of up to 16 hours.

3.6.2.1 Contingency Science

Several failures of MASCOT are under investigation and integrated into the failure analysis. Two major ones are the loss of GNC and the mobility, which would have direct consequences to the science operations of MASCOT. In a case of a GNC failure, in which day and night phases cannot be distinguished MASCOT can be operated via an on-board backup time timeline. Predefined timed payload operations can be scheduled in this case on a fixed timeline.
The MAG and MARA instruments will run continuously on this timeline and will be able to perform nominal operations. The MASCAM will be commanded in night mode all the time and MicroOmega will be scheduled in dedicated intervals in at least half of the nominal nighttime duration. The night mode operation of MASCAM during the entire MASCOT lifetime is secured by the LED measurements also if night rises or its FoV is in a shadowed area. The schedule of MicroOmega in dedicated timeframes related to the nominal night duration shall provide the opportunity for at least one night measurement. The data will be uplinked during each available link to the main spacecraft. In case MASCOT loses its self-rigthening functionality or losses of the ability to detect its orientation on the asteroid surface at least MAG can perform nominal operations as these are orientation independent. MARA and MASCAM measurements are dependent on the surface parts in their FoV. For MircOmega it would be important to have an orientation with its optical aperture is directed towards the surface. A data link of MASCOT to Hayabusa2 can be established in any orientation and the data will be uploaded and the commands can be received by MASCOT.

3.7 The First In Flight Activity

Since launch in 2014 several health checks and the first calibration campaign of the scientific payloads during cruise phase were conducted successfully. In addition, the launch locks (PRM) have been activated. MASCOT, its subsystems and scientific payloads, are in a good health state.

Acknowledgement

MASCOT was developed and built under the leadership of the German Aerospace Center (DLR) with contributions from the Centre National d'Études Spatiales (CNES) and Japan Aerospace Exploration Agency (JAXA).

Abbreviations

ADC	Analog-to-Digital Converter
CFRP	Carbon-Fiber-Reinforced Plastic
CoG	Center of Gravity
DC	Direct Current
E-box	Electronic Box
EM	Engineering Model
EQM	Engineering Qualitifaction Model
FM	Flight Model
FS	Flight Spare
FPGA	Field Programmable Gate Array
GNC	Guidance, Navigation and Control
HY2	Hayabusa2
LED	Light-Emitting Diode
MAM	MASCOT Autonomy Manager
MASCAM	MASCOT CAMera
MARA	MASCOT Radiometer
MASMAG	MASCOT MAGnetometer
MLI	Multi Layer Insulation
MOSFET	Metal-Oxide-Semiconductor Field-Effect Transistor
MSC	MASCOT
NEA	Non Explosive Actuator
OBC	On-board Computer
PCDU	Power Conditioning and Distribution Unit
PCB	Printed Circuit Boa
SAR	Safe Activation Relay
SLI	Single Layer Insulator
UMC	Umbilical Separation Connecter

References

M. Abe, Y. Takagi, K. Kitazato, S. Abe, T. Hiroi, F. Vilas, B.E. Clark, B. P.A. Abell, S. M. Lederer, K.S. Jarvis, T. Nimura, Y. Ueda, A. Fujiwara, Near-Infrared Spectral Results of Asteroid Itokawa from the Hayabusa Spacecraft, Science (312), 1334 (2006).

A. Accomazzo, P. Ferri, S. Lodiot et al., Rosetta operations at the comet, Acta Astronautica, Vol 115, pp. 434-441, 2015

M. F. A'Hearn, M. J. S. Belton, A. Delamere, W. H. Blume, Deep Impact: A Large-Scale Active Experiment on a Cometary Nucleus, Space Science Reviews, **117**, 1 (2005a)

M.F. A'Hearn, M. J. S.; Belton, W.A. Delamere, J. Kissel, K.P. Klaasen, L.A. McFadden, K.J. Meech, H.J. Melosh, P.H. Schultz, J.M. Sunshine, P.C. Thomas, J. Veverka, D.K. Yeomans, M.W. Baca, I. Busko, C.J. Crockett, S.M. Collins, M. Desnoyer, C.A. Eberhardy, C.M. Ernst, F.L. Farnham, L. Feaga, O. Groussin, D. Hampton, S.I. Ipatov, J-Y. Li, D. Lindler, C.M. Lisse, C. N. Mastrodemos, W.M. Owen, J.E. Richardson, D.D. Wellnitz, R.L. White, Deep Impact: Excavating Comet Tempel 1, Science, **310**, 258 (2005b)

Barucci, M. A., Cheng, A. F., Michel P., Benner, L. A. M., Binzel R. P., Bland, P. A. Böhnhardt, H., Brucato, J. R., Campo Bagatin, A., Cerroni, P., Dotto, E., Fitzsimmons, A., Franchi I., Green S. F., Lara, L.-M., Licandro, J., Marty, B., Muinonen, K., Nathues, A., Oberst, J., Rivkin, A. S., Robert, F., Saladino, R., Trigo-Rodriguez, J.M., Ulamec, S. and Zolensky, M., MarcoPolo-R near earth asteroid sample return mission; *Exp. Astronomy*, Vol. 33, No. 2-3, pp. 645-684, 2012

Biele, J., Ulamec, S. Capabilities of Philae, the Rosetta Lander. Space Sci. Rev. 138, 275–289, 2008

J. Biele, S. Ulamec, M. Maibaum, R. Roll, L. Witte, J. Pablo Muñoz, W. Arnold, H.-U. Auster, C. Casas, C. Faber, C. Fantinati, F. Finke, H.-H. Fischer, K. Geurts, C. Güttler, P. Heinisch, A. Herique, S. Hviid, G. Kargl, M. Knapmeyer, J. Knollenberg, W. Kofman, N. Kömle, E. Kührt, V.Lommatsch, S. Mottola, R. P. de Santayana, E. Remetean, F. Scholten, K. Seidensticker, H. Sierks and T. Spohn, The landing(s) of Philae and inferences about comet surface mechanical properties. *Science* 349, aaa9816, 2015

D.E. Brownlee, F. Horz, R.L. Newburn, M. Zolensky, T. Duxbury, C. Thomas, S. Sandford, Z. Sekanina, P. Tsou, M. Hanner, Martha B.C. Clark, S.F. Green, J. Kissel, Surface of Young Jupiter Family Comet 81 P/Wild 2: View from the Stardust Spacecraft, Science, **304**, 1764 (2004)

Cho, Y. I., Thermal Modeling of High Rate Li-SOCl2 Primary Cylindrical Cells. Journal of The Electrochemical Society 134(4): 771-779, 1987.

E.T. Eisenmann, Lithium – Thionyl Chloride Battery State-of-the-Art Assessment, Sandia Report SAND96-0839 • UC-400, March 1996.

T. Evans, T. Nguyen, et al. A mathematical model of a lithium/thionyl chloride primary cell. Journal of The Electrochemical Society 136(2): 328-339, 1989.

M. Grott , J. Knollenber, B. Borgs, F. Hänschke, E. Kessler, J. Helbert, A. Maturilli, N. Müller The MASCOT Radiometer MARA for the Hayabusa 2 Mission, This Special Issue

A. Fujiwara, J. Kawaguchi, D.K. Yeomans, M. Abe, T. Mukai, T. Okada, J. Saito, H. Yano, M. Yoshikawa, D.J. Scheeres, O. Barnouin-Jha, A. F. Cheng, H. Demura, R.W. Gaskell, N. Hirata, H. Ikeda, T. Kominato, H. Miyamoto, A.M. Nakamura, R. Nakamura, S. Sasaki, K. Uesugi, The Rubble-Pile Asteroid Itokawa as Observed by Hayabusa, Science, **312,** 1330 (2006).

Glassmeier, K.-H., Bo¨hnhardt, H., Koschny, D., Ku¨ hrt, E., Richter, I.
The Rosetta Mission. Flying towards the Origins of the Solar System., Space Sci. Rev. 128, 1–21, 2007.

J.T. Grundmann, J. Biele, R. Findlay, S. Fredon, T.-M. Ho, C. Krause, S. Ulamec, C. Ziach, One Shot to an Asteroid – MASCOT and the Design of an Exclusively Battery Powered Small Spacecraft in Hardware Design Examples and Operational Consideration, European Space Power Conference 2014, #3051.

D. Hercik, H.-U. Auster, J. Blum, K.-H. Fornacon, M. Fujimoto, K. Gebauer, C. Guttler, O. Hillenmaier, A. Hördt, I. Richter, B. Stoll, B. Weiss, K.-H. Glaßmeier, MasMag: The MASCOT Magnetometer experiment, This Special Issue (2015)

Jaumann et al. (2014)

R. Jaumann, N. Schmitz, A. Koncz, H. Michaelis, S. Schroeder, S. Mottola, F. Trauthan, H. Hoffmann, T. Roatsch ,D. Jobs, J. Kachlicki, B. Pforte, R. Terzer, M. Tschentscher, S. Weisse, U. Mueller, T.-M. Ho, M. Grott, J.P. Bibring, J. Biele, S. Ulamec, B. Broll, A. Kruselburger, L. Perez-Prieto, The camera of the MASCOT asteroid lander on board Hayabusa-2 , This Special Issue (2015)

Joos, H.-D. ; Bals, J. ; Looye, G. ; Schnepper, K. ; Varga, A: A multiobjective optimisation-based software environment for control sys-tems design. In: IEEE International Conference on Control Applications and International Symposium on Computer Aided Control Systems Design, Glasgow, Scotland, UK, S. 7-14, 2002

H.U. Keller, C. Arpigny, C Barbieri, R.M. Bonnet, S. Cazes, M. Coradini, C.B. Cosmovici, W.A. Delamere, W.F. Huebner, D.W. Hughes, C. Jamar, D. Malaise, H.J. Reitsema, H. U. Schmidt, W.K.H. Schmidt, P. Seige, F.L. Whipple, K. Wilhelm, First Halley multicolour camera imaging results from Giotto, Nature, **321**, 326 (1986).

M. Lange, O. Mierheim, C. Hühne. MASCOT - Structures Design and Qualification of an "Organic" Mobile Lander Platform for Low Gravity Bodies. Proc. of '13th European Conference on Space Structures, Materials & Environmental Testing', Braunschweig, Germany, ESA SP-727 (2014)

Lange, M. et al. MASCOT - A Lightweight Multi-Purpose Lander Platform. Proc. of '12th European Conference on Space Structures, Materials & Environmental Testing', Noordwijk, The Netherlands, ESA SP-691 (2012)

Lauretta D.S. and the OSIRIS-REx Team, An overview of the OSIRIS-Rex asteroid sample return mission, 43rd Lunar and Planetary Science Conference, # 2491 (2012)

Lichtenheldt, R. ; Schäfer, B.: Hammering beneath the Surface of Mars - Modellbildung und Optimierung des HP3-Mole. In: in L. Zentner (Hrsg.): 10. Kolloquium Getriebetechnik, S.169-186, ISBN 978-3-86360-065-5, Ilmenau, 2013

Lichtenheldt, R., Spytek, J. and Reill, J.: Coaching Mascot for broad-jumping: Multi-criterial optimization of the arm trajectories for Mascot's hopping locomotion, 11th Low-cost Planetary Mission Conference, Berlin, 2015

T. Okada, K. Shirai, Y. Yamamoto, T. Arai, K. Ogawa, K. Hosono, M. Kato, X-ray Fluorescence Spectrometry of Asteroid Itokawa by Hayabusa, Science, **312**, 1338, (2006).

Reinhard et al., Nature, vol 321 p313

J. Saito, H. Miyamoto, R. Nakamura, M. Ishiguro, T. Michikami, A.M. Nakamura, H. Demura, S. Sasaki, N. Hirata, C. Honda, A. Yamamoto, Y. Yokota, T. Fuse, F. Yoshida, D.J. Tholen, R.W. Gaskell, T. Hashimoto, T. Kubota, Y. Higuchi, T. Nakamura, P. Smith, K. Hiraoka, T. Honda, S. Kobayashi, M. Furuya, N. Matsumoto, E. Nemoto, A. Yukishita, K. Kitazato, B. Dermawan, A. Sogame, J. Terazono, C. Shinohara, H. Akiyama, Detailed Images of Asteroid 25143 Itokawa from Hayabusa, Science, **312**, 1341 (2006).

R.Schulz, C.Alexander, H. Böhnhardt, K.-H.Glaßmeier (Eds.), Rosetta—ESA's Mission to the Origin of the Solar System, Springer, ISBN: 978-0-387-77517-3, 2009

M. Schlotterer, R. Findlay, Ross, T.M. Ho, L. Witte, C. Ziach, Histogram Filter for Attitude Determination of Small Asteroid Lander, In: 9th International ESA Conference on Guidance, Navigation & Control Systems. 9th International ESA Conference on Guidance, Navigation & Control Systems, 2.-6. Juni 2014, Porto, Portugal.

P. H. Schultz, C. A. Eberhardy, C. M. Ernst, M. F. A'Hearn, J. M. Sunshine, C. M. Lisse, The Deep Impact oblique impact cratering experiment, Icarus, **191**, 84 (2007)

H. Sierks, C. Barbieri, P. L. Lamy, R. Rodrigo, D. Koschny, H. Rickman, H. U. Keller, J. Agarwal, M. F. A'Hearn, F. Angrilli, A.-T. Auger, M. A. Barucci, J.-L. Bertaux, I. Bertini, S. Besse, D. Bodewits, C. Capanna, G. Cremonese, V. Da Deppo, B. Davidsson, S. Debei, M, De

Cecco, F. Ferri, S. Fornasier, M. Fulle, R. Gaskell, L. Giacomini, O. Groussin, P. Gutierrez-Marques, P. J. Gutiérrez, C. Güttler, N. Hoekzema, S. F. Hviid, W.-H. Ip, L. Jorda, J. Knollenberg, G. Kovacs, J. R. Kramm, Ekkehard Kührt, M. Küppers, F. La Forgia, L. M. Lara, M. Lazzarin, C. Leyrat, Josè J. Lopez Moreno, S. Magrin, S. Marchi, F. Marzari, M. Massironi, H. Michalik, R. Moissl, S. Mottola, G. Naletto, N. Oklay, M. Pajola, M. Pertile, F.Preusker, L. Sabau, F. Scholten, C. Snodgrass, N. Thomas, C. Tubiana, J.B. Vincent, K.P. Wenzel, M. Zaccariotto, M. Pätzold, On the nucleus structure and activity of comet 67P/Churyumov-Gerasimenko, Science, **347**, 6220, (2015)

R.M. Spotnitz, G.S. Yeduvaka, G. Nagasubramanian, R. Jungst, Modeling self-discharge of Li/SOCl2 cells, Journal of Power Sources, **163**, 578 (2006)

J. M. Sunshine, O. Groussin, Peter H. Schultz, Michael F. A'Hearn, Lori M. Feaga, Tony L. Farnham, Kenneth P. Klaasen, The distribution of water ice in the interior of Comet Tempel 1, Icarus, 191, 73 (2007).

Tsuda, Y., M. Yoshikawa, M. Abe, H. Minamino, S. Nakazawa, System design of the Hayabusa2 - Asteroid sample return mission to1999JU3. Acta Astronautica. 91, 356-362, 2013.

S.Ulamec ,J.Biele, Surface elements and landing strategies for small bodies missions—Philae and beyond,Adv.SpaceRes.47, pp. 847–858, 2009

Ulamec, S., Biele, J., Bousquet, P.-W., Gaudon, P., Geurts, K., Ho, T.-M., Krause, C., Lange, C., Willnecker, R. and Witte L.; Landing on Small Bodies: From the Rosetta Lander to MASCOT and beyond; *Acta Astronautica*, Vol. 93, pp. 460-466, 2014

Veverka, J., Belton, M., Klaasen, K., Chapman, C. Galileo's Encounter with 951 Gaspra: overview. Icarus 107 (1), 2–17, 1994.

T. Yoshimitsu, T. Kubota, I. Nakatani, The opearation and scientific data of MINERVA rover in Hayabusa mission, 36th COSPAR Scientific Assembly, #2987, 2006

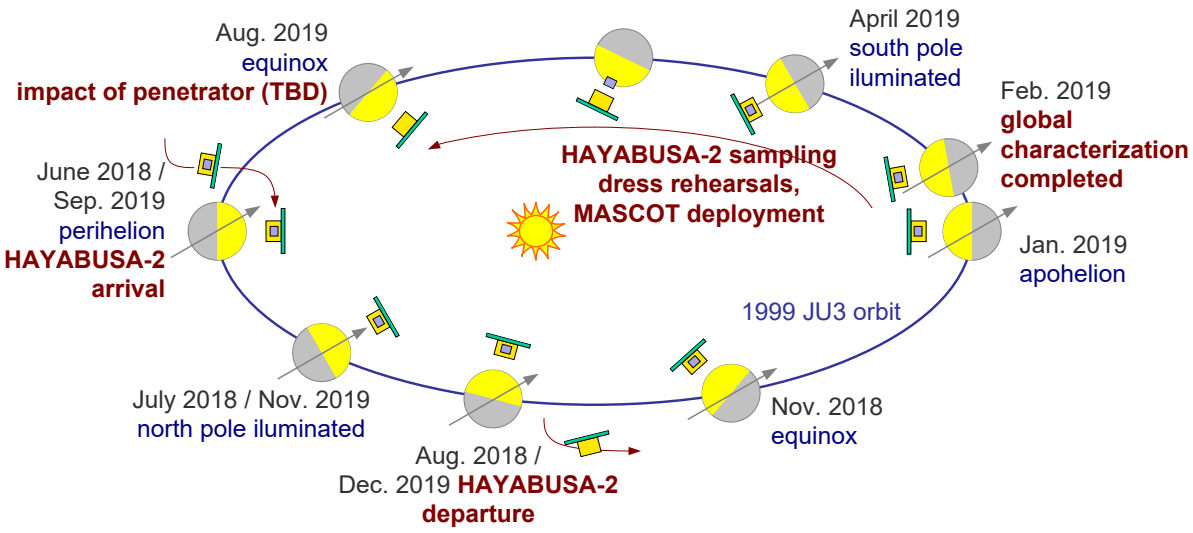

Figure 1: HAYABUSA2 Mission Baseline.

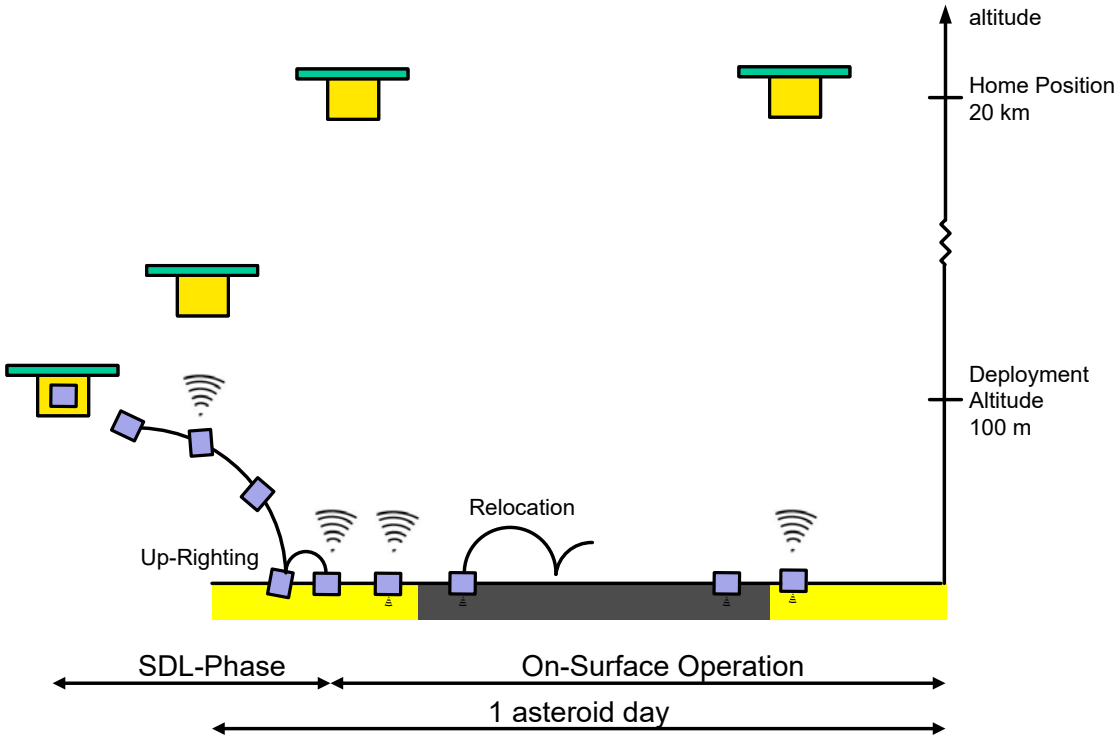

Figure 2: The 'on-asteroid' surface operation baseline of the MASCOT lander

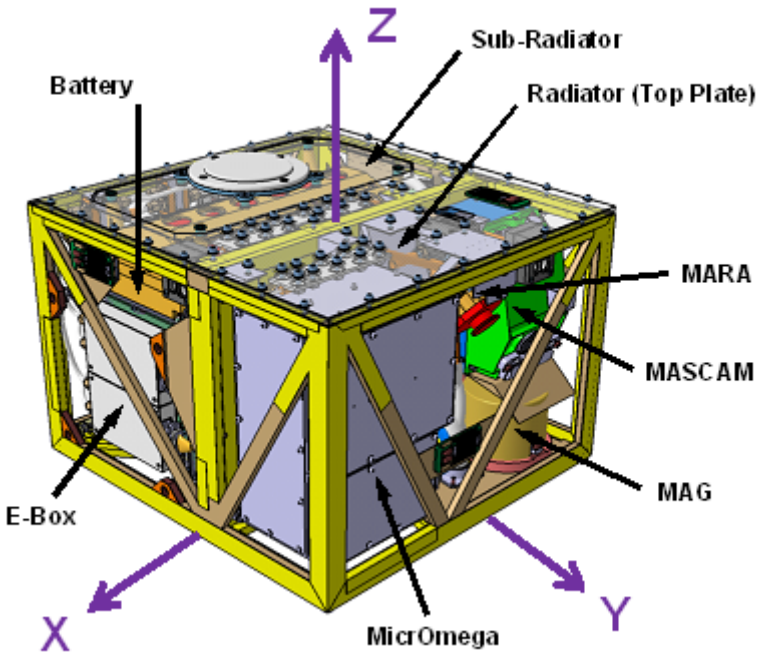

Figure 3: MASCOT Lander Module.

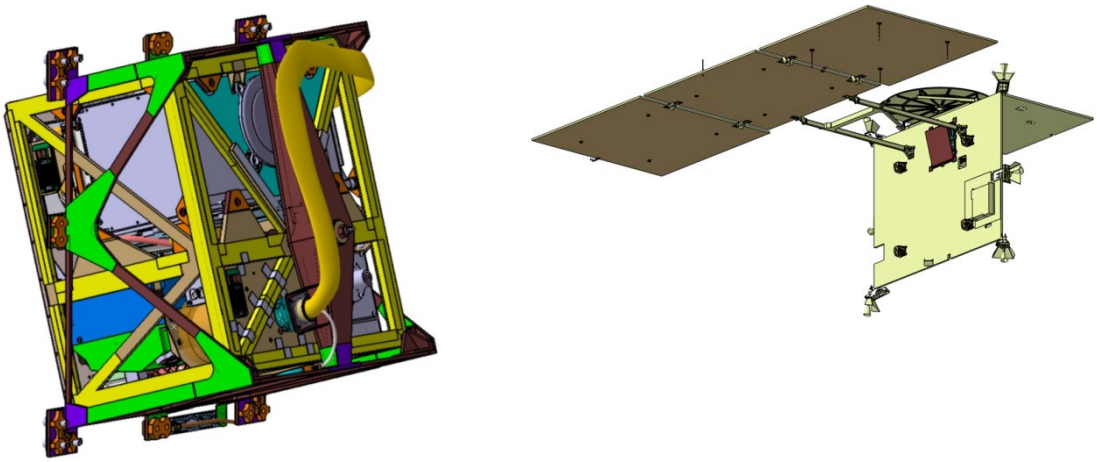

Figure 4: MASCOT and MESS (left). MASCOT attached on the –Y panel of the HY2 spacecraft (right).

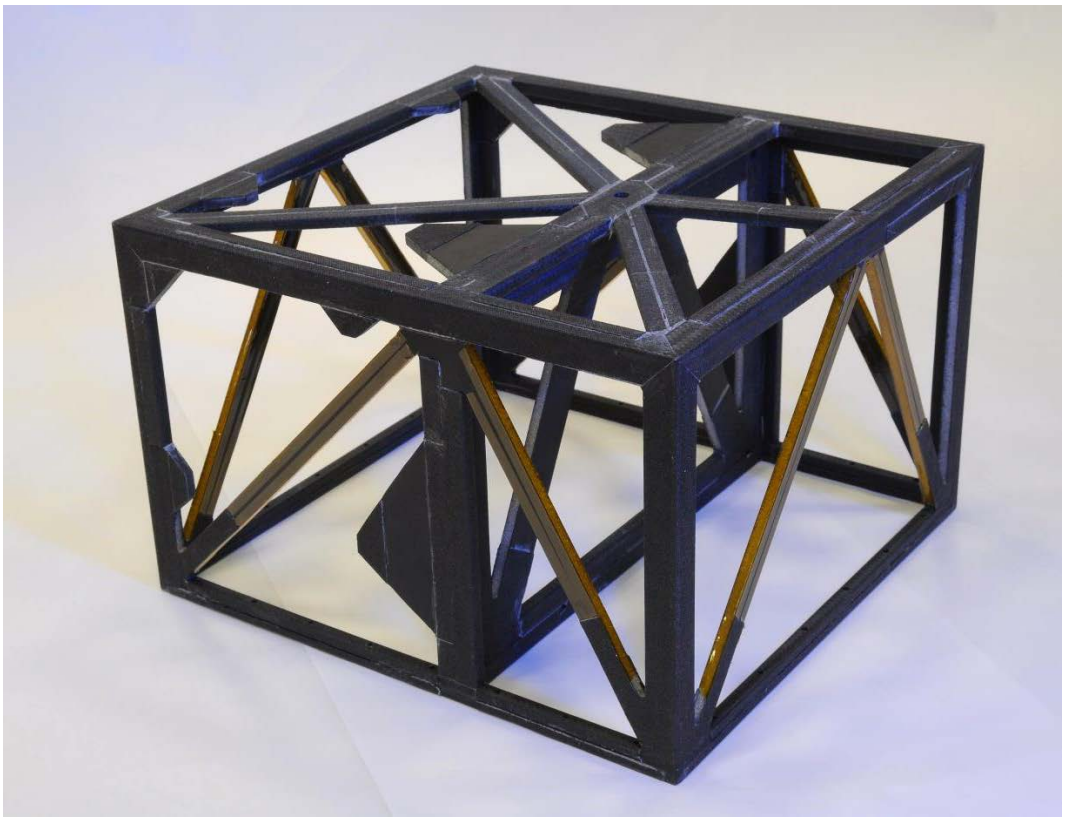

Figure 5: MASCOT Lander Module structure STM2.2 (bottom up).

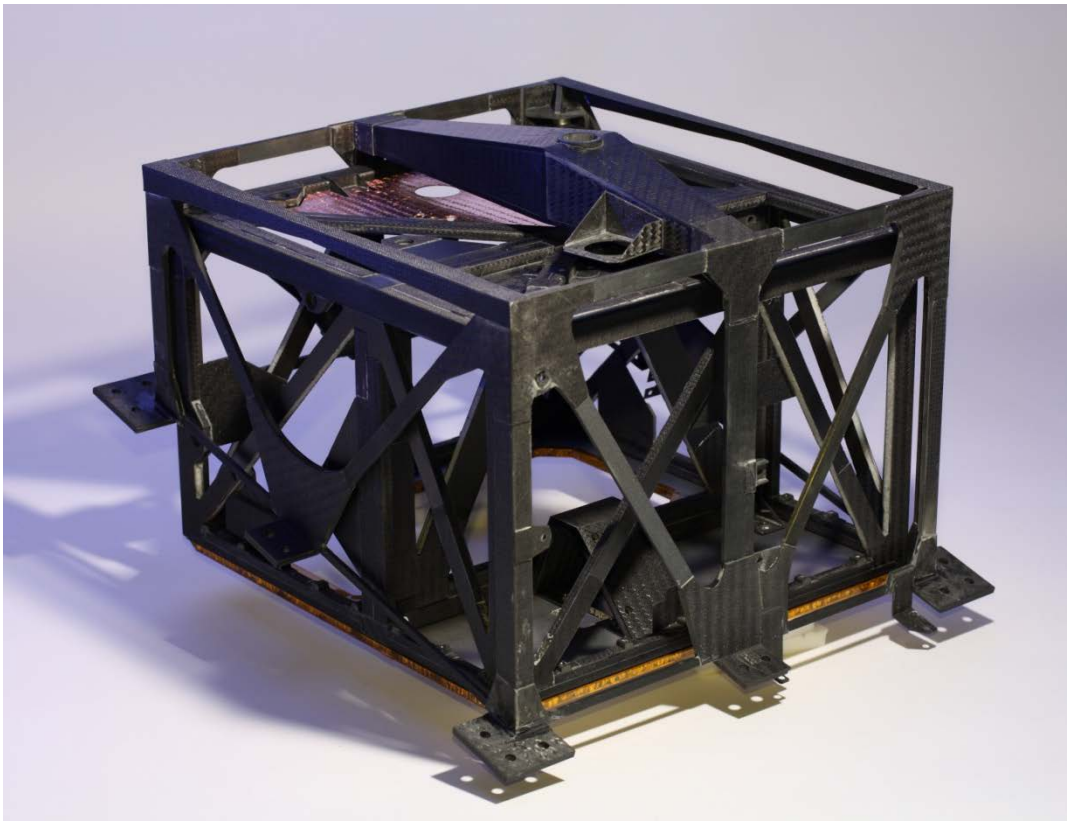

Figure 6: MASCOT Lander Module FM structure inside of the MESS FM structure.

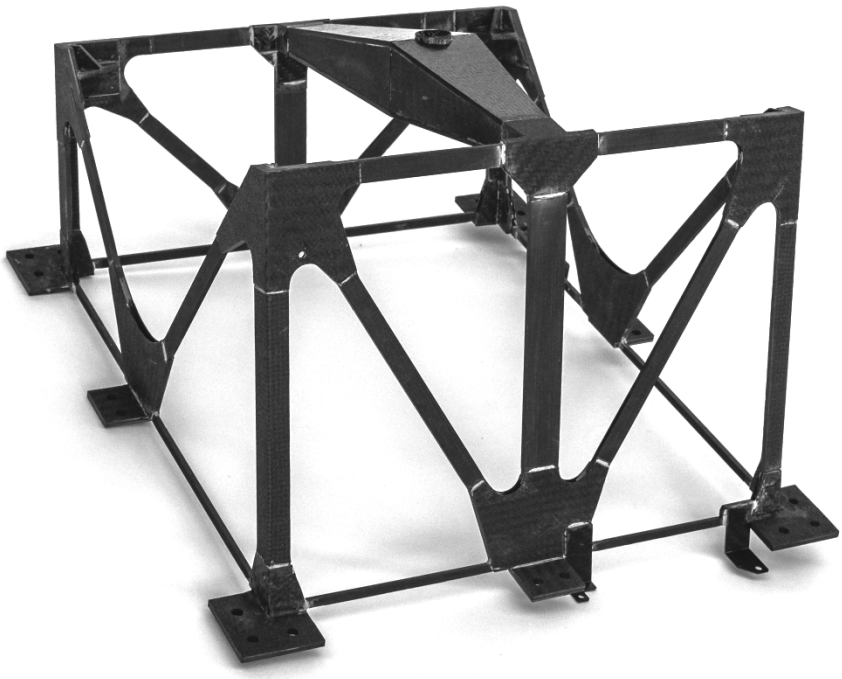

Figure 7: MESS STM structure with location of details in following figure.

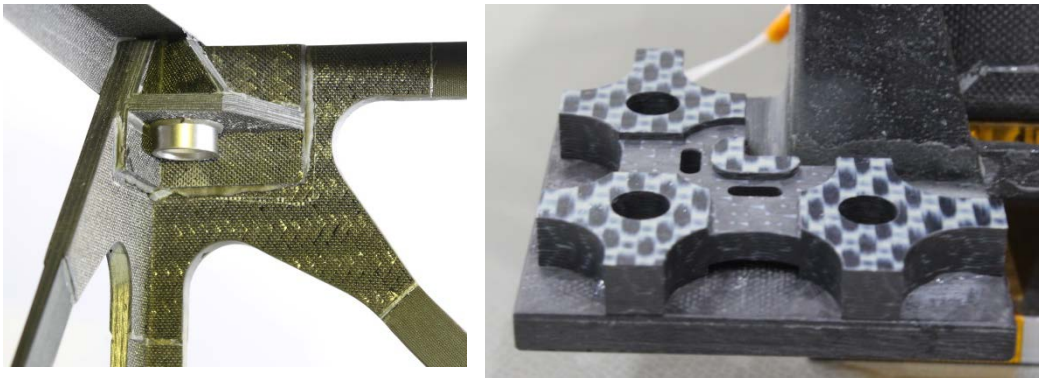

Figure 8: Details of MESS FM bearing corner (left) and MESS FM feet insulator made of fiber-reinforced PEEK (right).

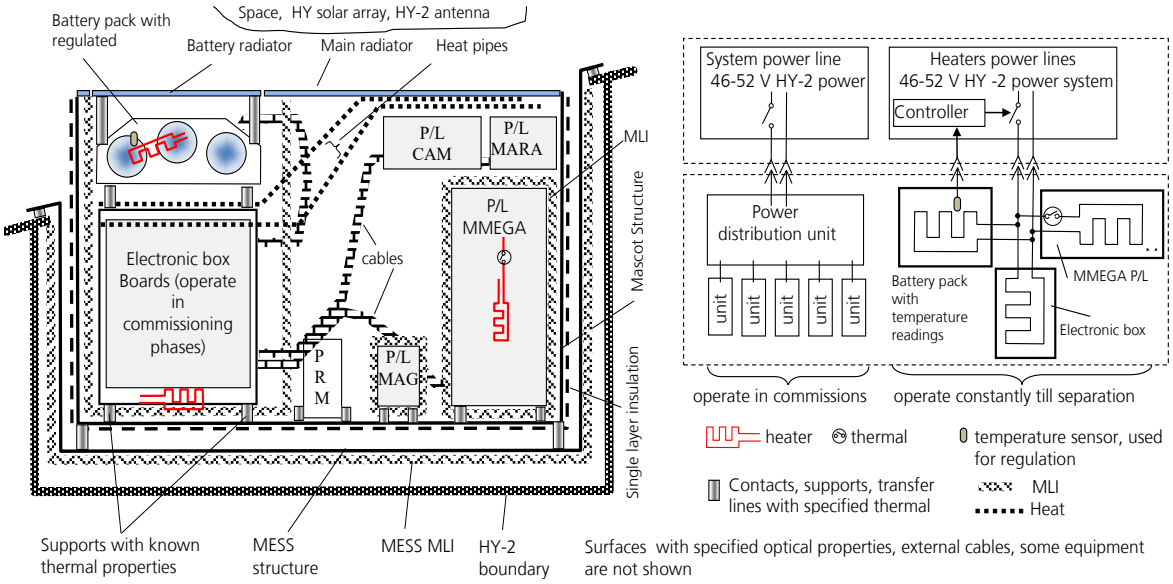

Figure 9: Structure of MASCOT thermal control system (left); heating power distribution and heaters lines (right). All controlling lines are redundant. MESS structure, MESS MLI will be the part of HY2 spacecraft after MASCOT separation

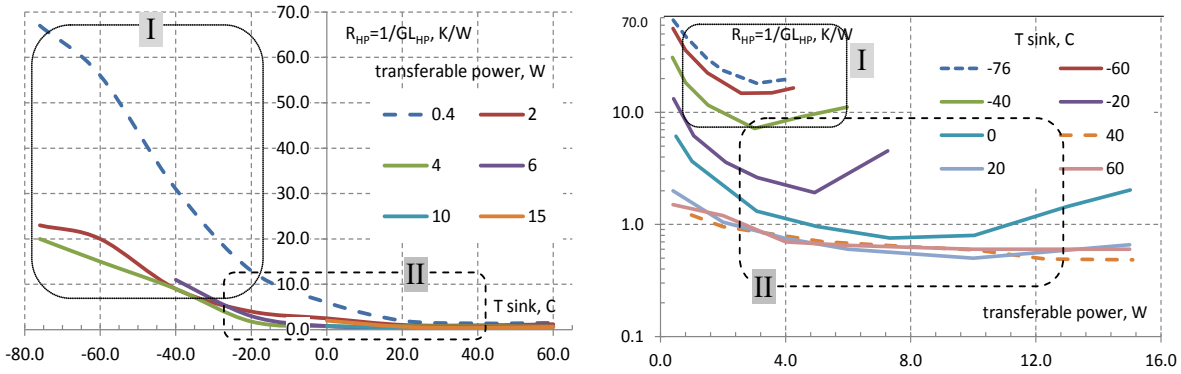

Figure 10: Heat pipes performance: thermal resistance as the function of heat sink temperature with stratification on transferred power (a) and transferred power with stratification on heat sink temperature (b). I, II – approximate areas of operation in cruise and on asteroid surface correspondently

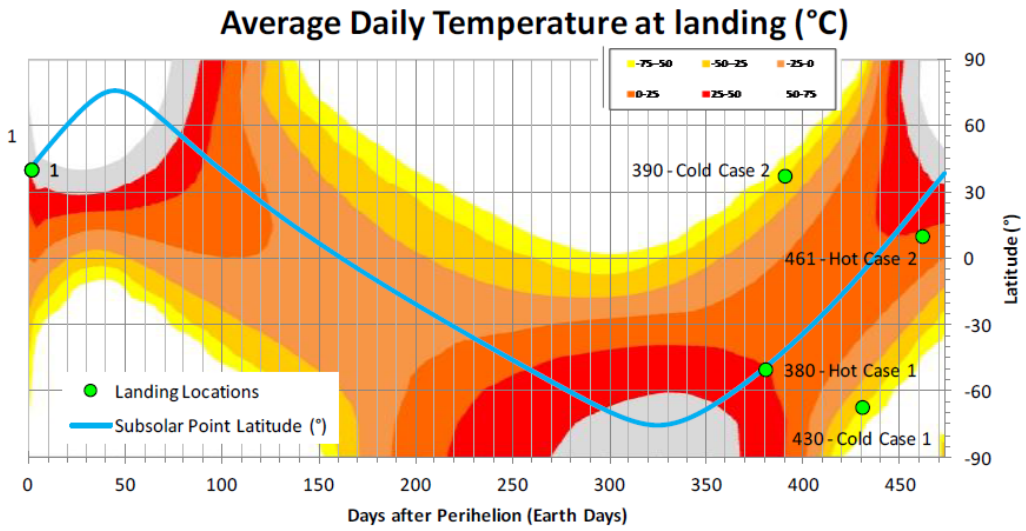

Figure 11: Possible MASCOT landing locations on the asteroid surface. Averaged per asteroid day temperature pattern is shown

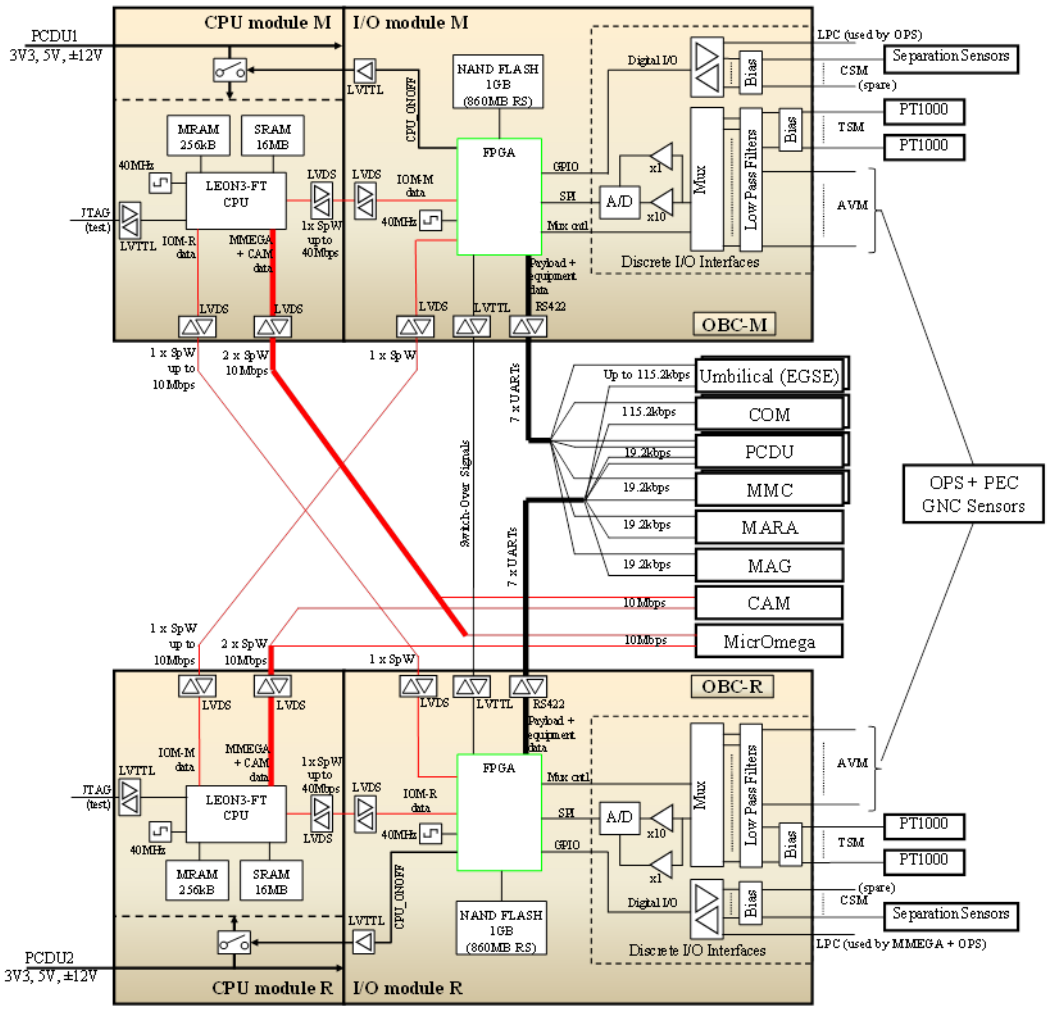

Figure 12: MASCOT OBC Schematics

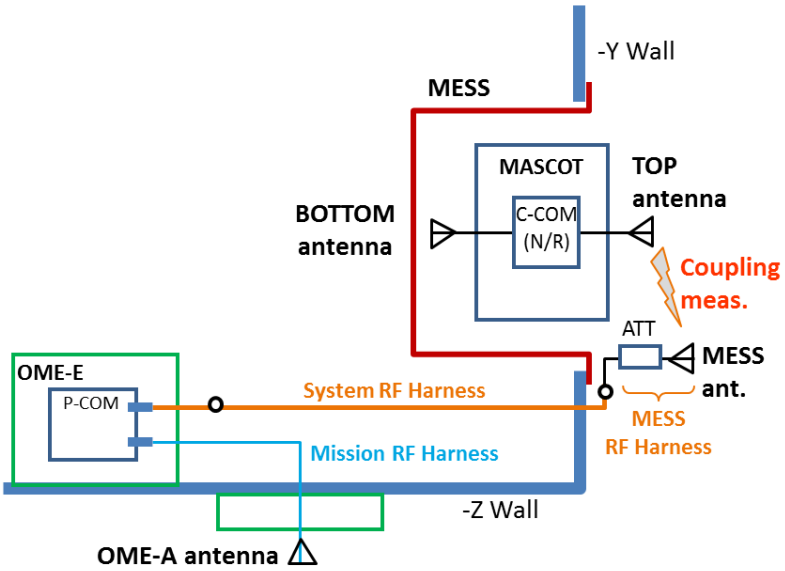

Figure 13: RF communication chains between MASCOT and HY 2

Figure 14: CCOM transceiver overview

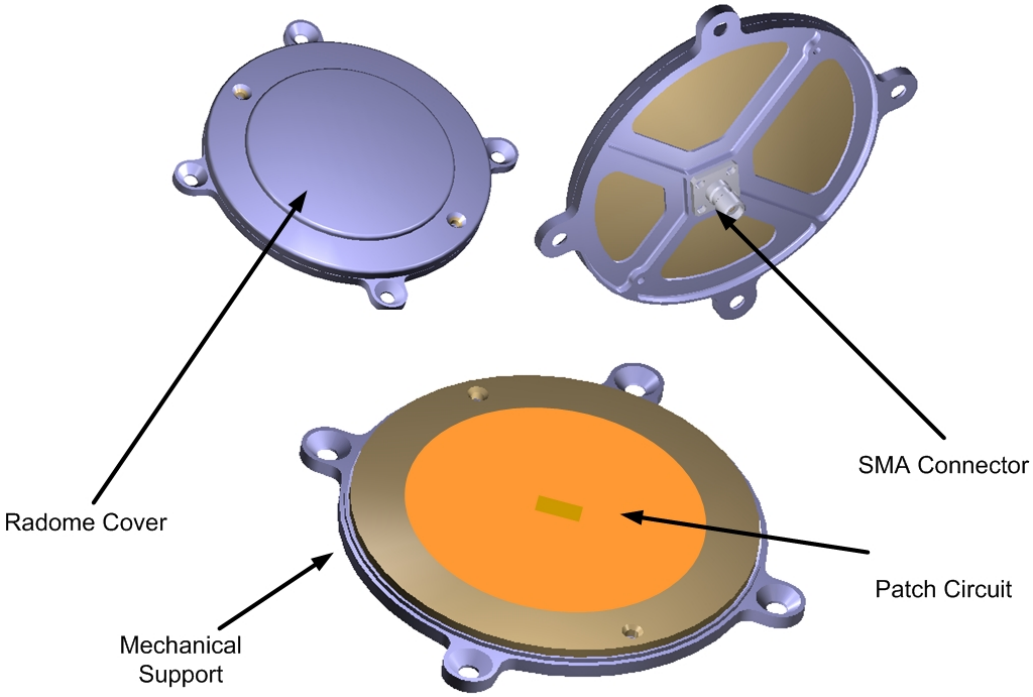

Figure 15 : MASCOT antennas

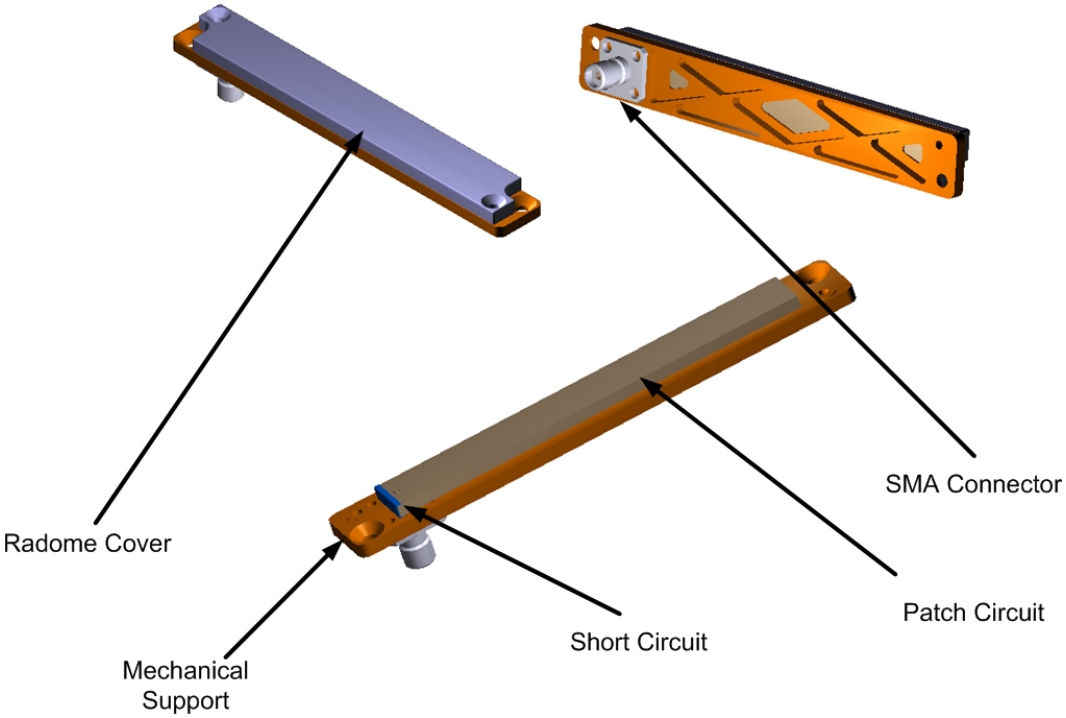

Figure 16 : MESS Antenna

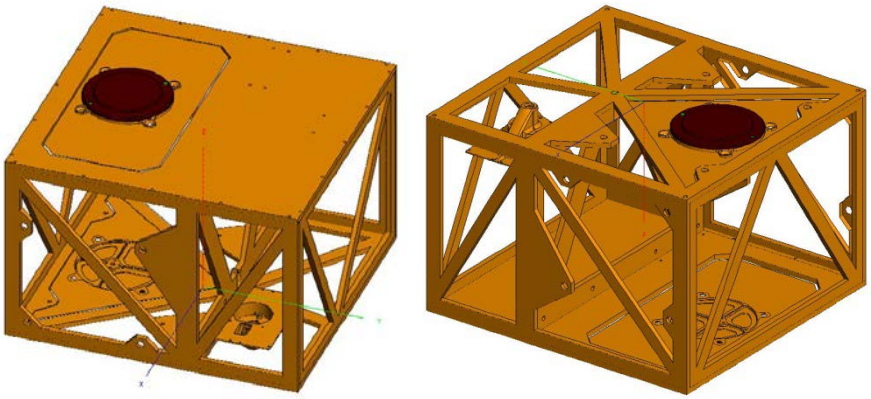

Figure 17 : MASCOT antennas optimized on structure by EM simulation

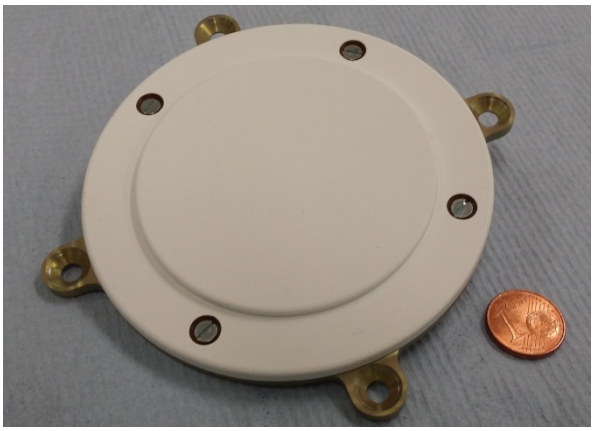

Figure 18 : MASCOT Antenna Flight Model

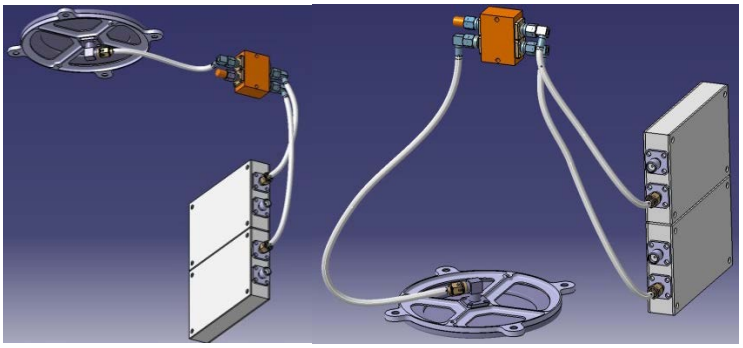

Figure 19 : MASCOT RF Harness.

Figure 20: FM Battery of the MSC lander, top side (left) and bottom side (right).

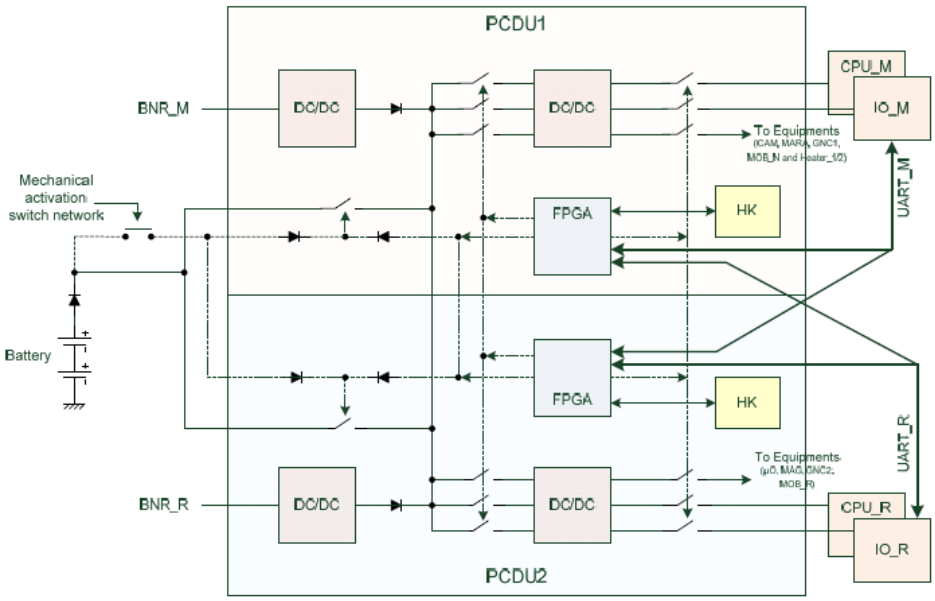

Figure 21: MASCOT PCDU architecture (top).

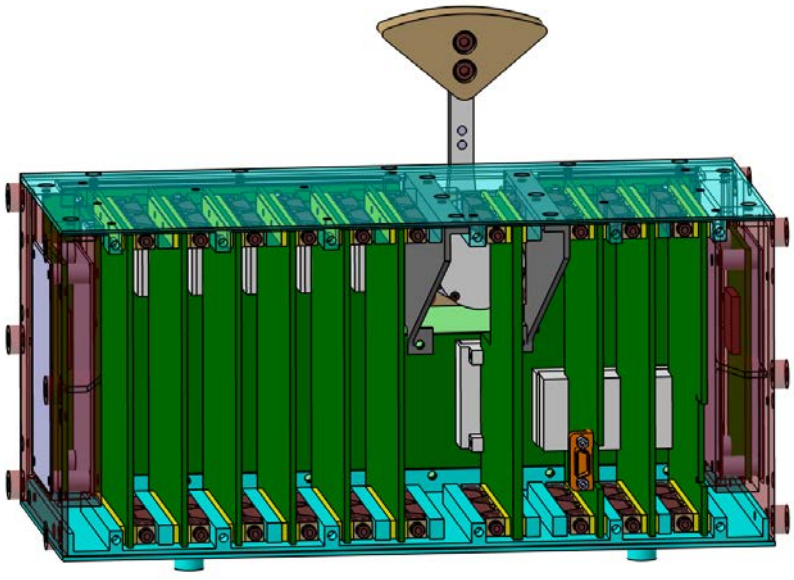

Figure 22: MASCOT E-Box Backplane & Cards.

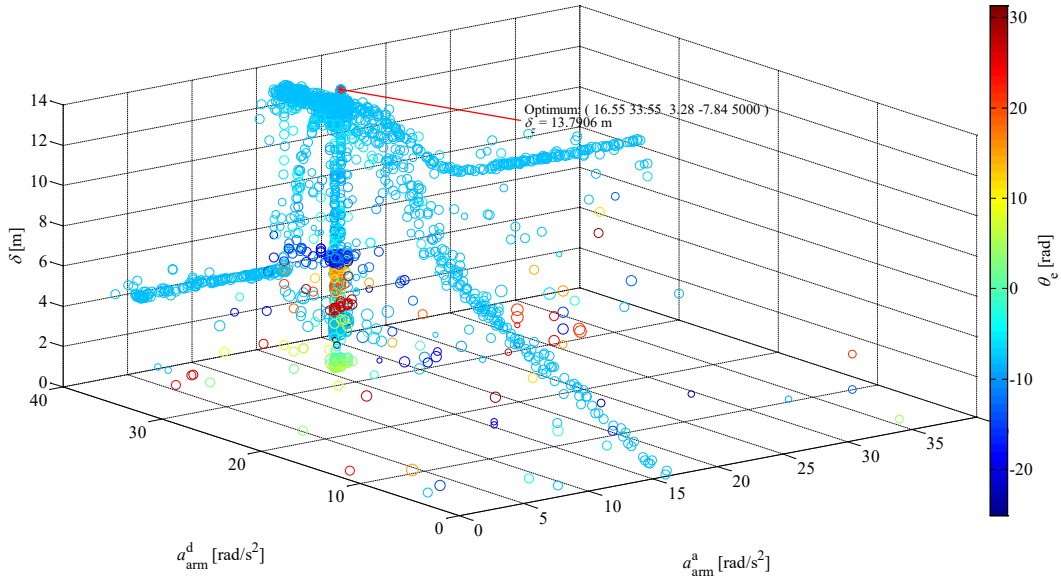

Figure 23: Jumping distance up to the first ground contact – path through 4 dimensional parameter space; coloring shows the arm end angle and marker size is correspondent to the initial arm angle [3]

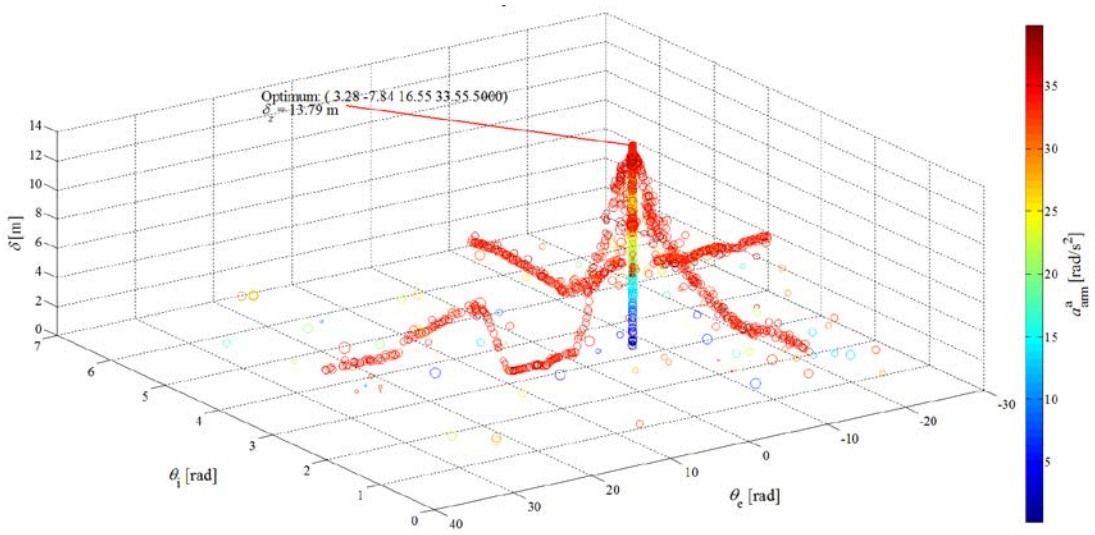

Figure 24: Jumping distance up to the first ground contact – path through 4 dimensional parameter space; coloring shows the arm deceleration and marker size is correspondent to arm acceleration [3]

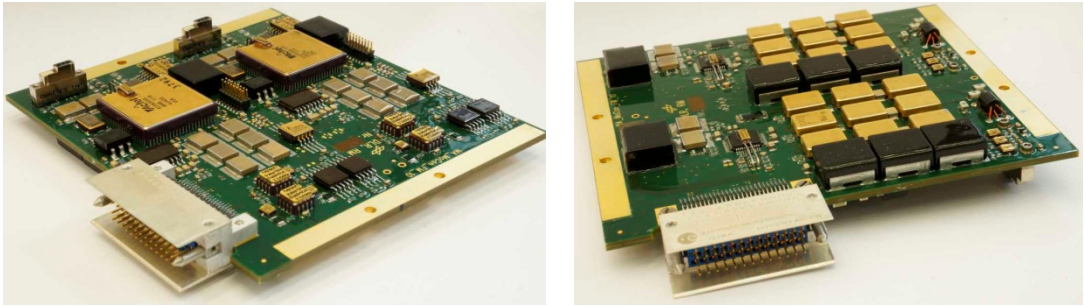

Figure 25: Photo images of mobility flight model electronics PCB (on the left: top side, on the right: bottom side).

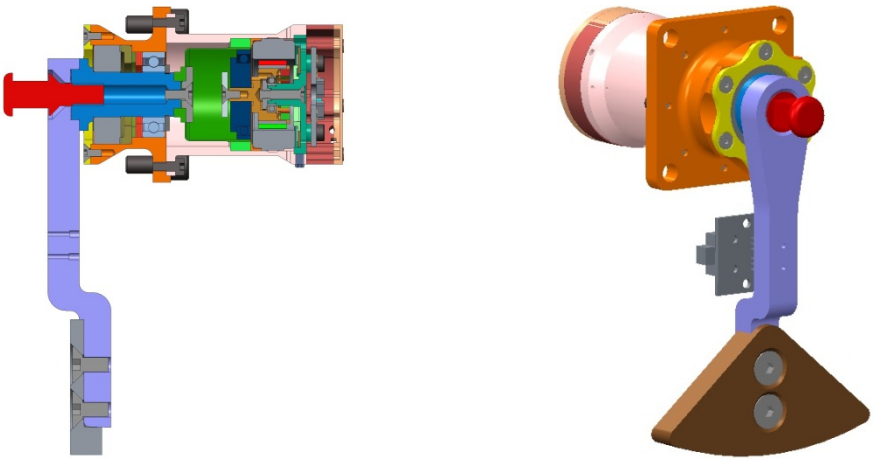

Figure 26: On the left: CAD sectional drawing of mobility unit (MobUnit) showing the compact fusion of Harmonic Drive gearing with brushless DC motor. On the right: CAD image of motor and eccentric arm.

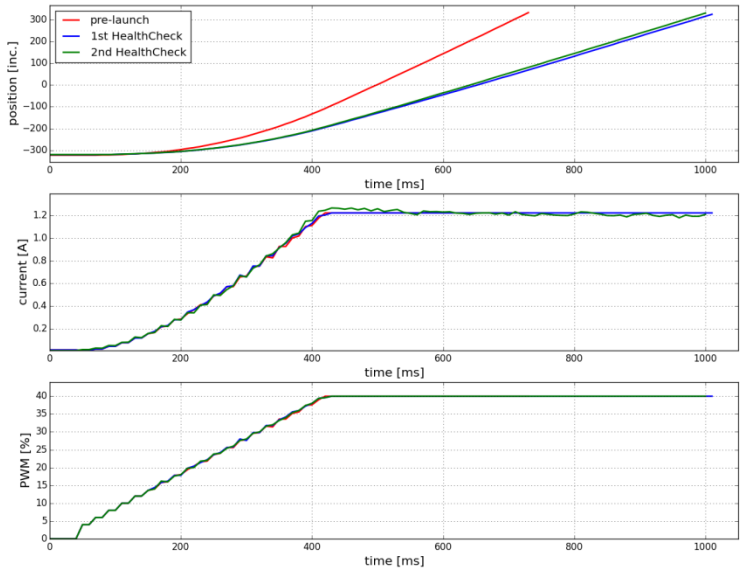

Figure 27: Comparison of health check data measured before launch (red) and during cruise phase (blue and green).

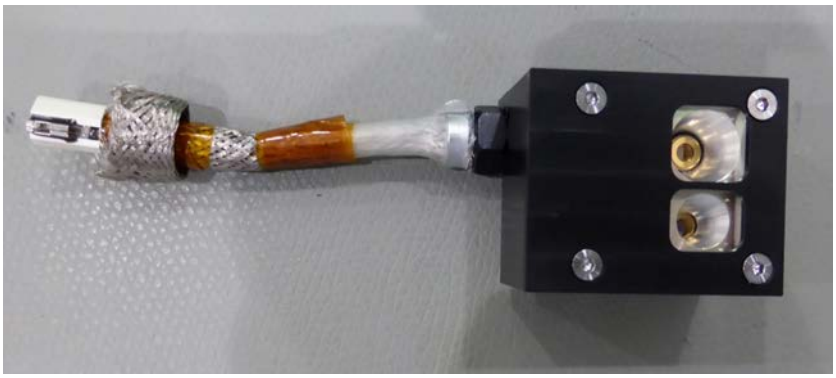

Figure 28: Optical Proximity Sensor (OPS)

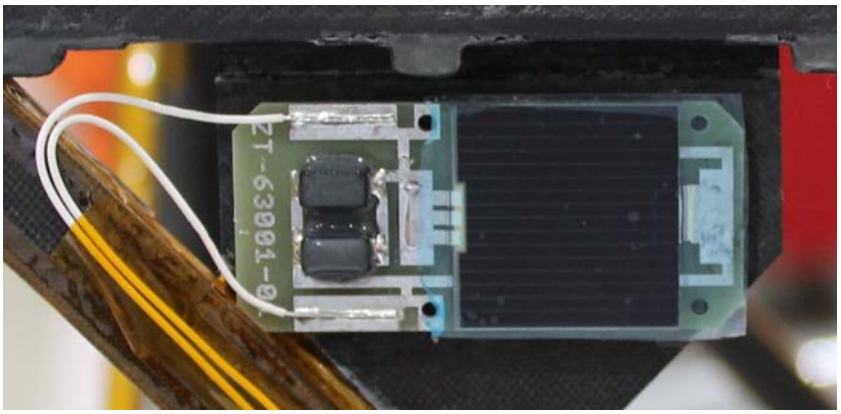

Figure 29: Photoelectric Cell Sensor (PEC) glued to MASCOT surface.

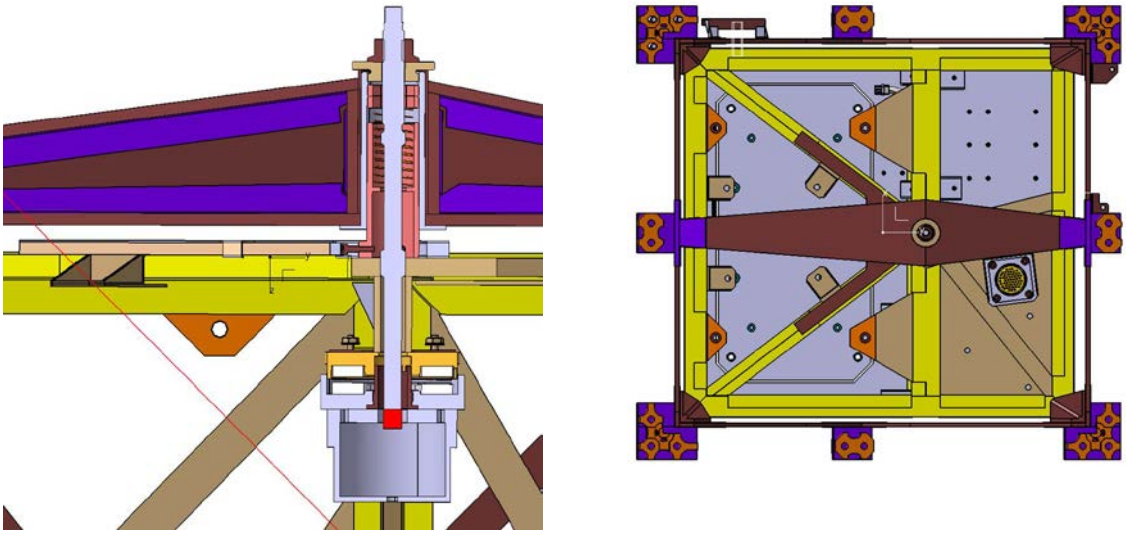

Figure 30: Overview of separation mechanism

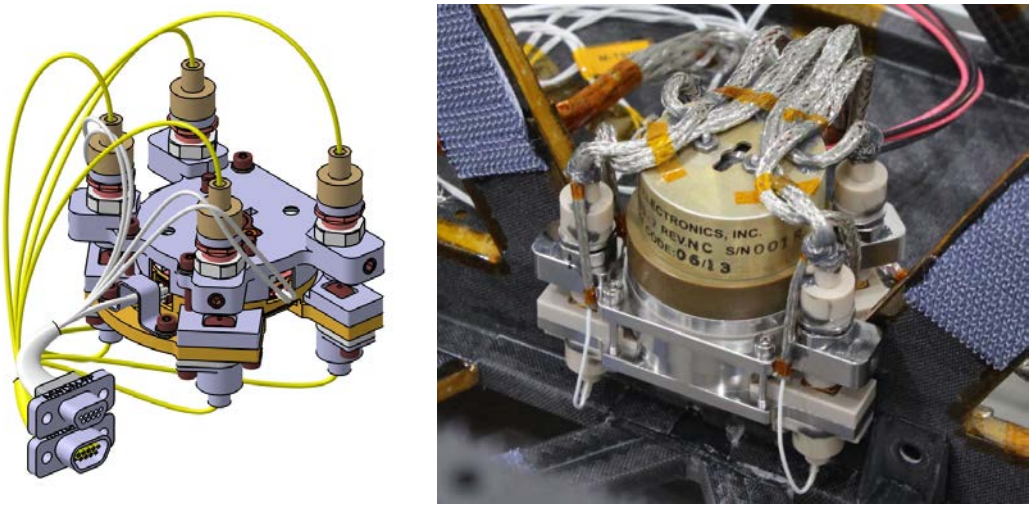

Figure 31: Sketch of PRM CAD design (left) and FM model integrated in the structure (right).

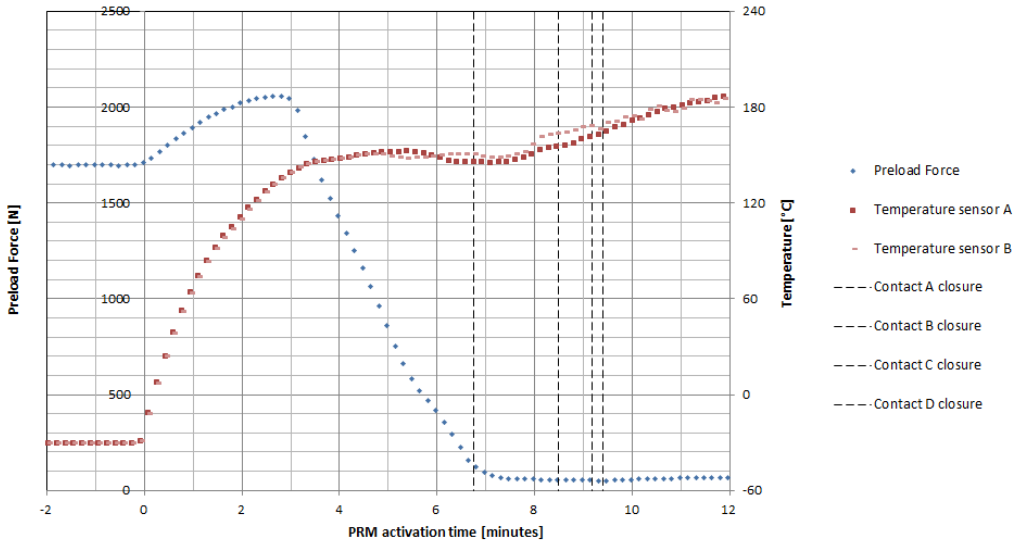

Figure 32: The remaining preload force and PRM temperature during a melting process.

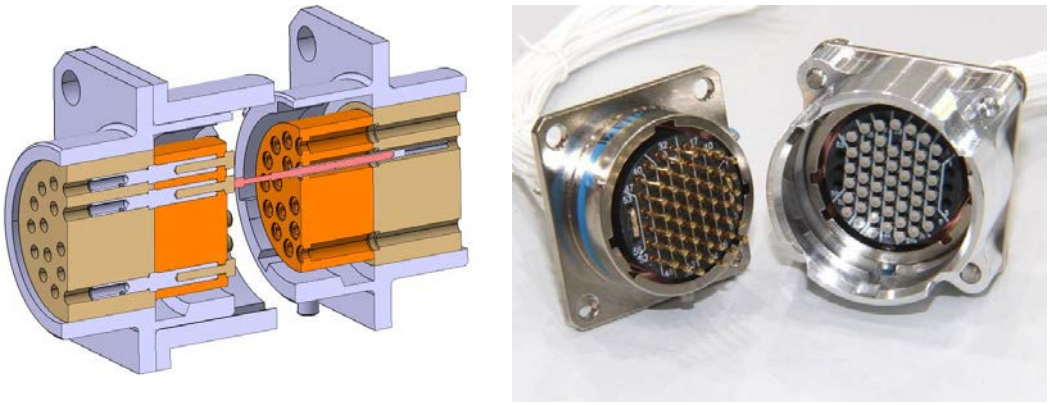

Figure 33: Sketch of Umbilical (left) and Flight Model (right).

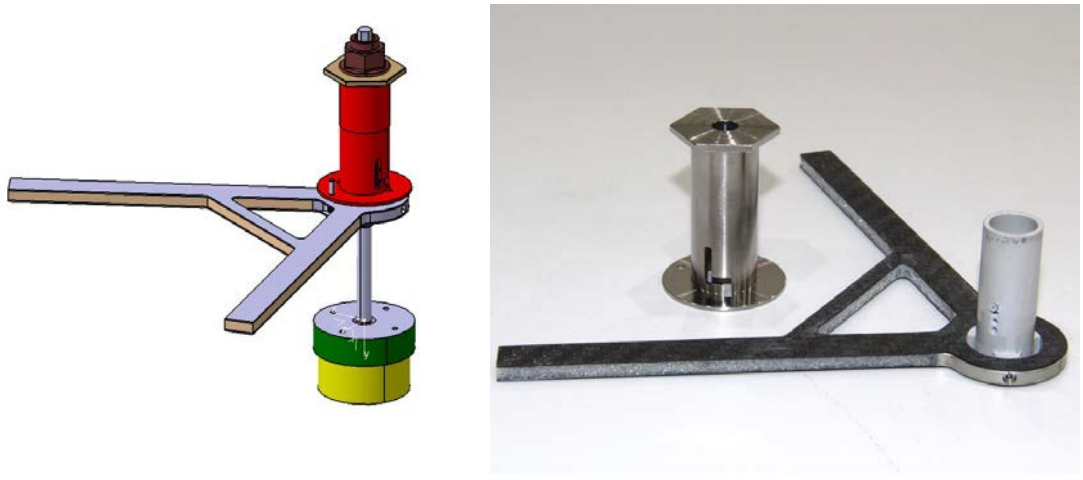

Figure 34: Push of plate of the separation mechanism.

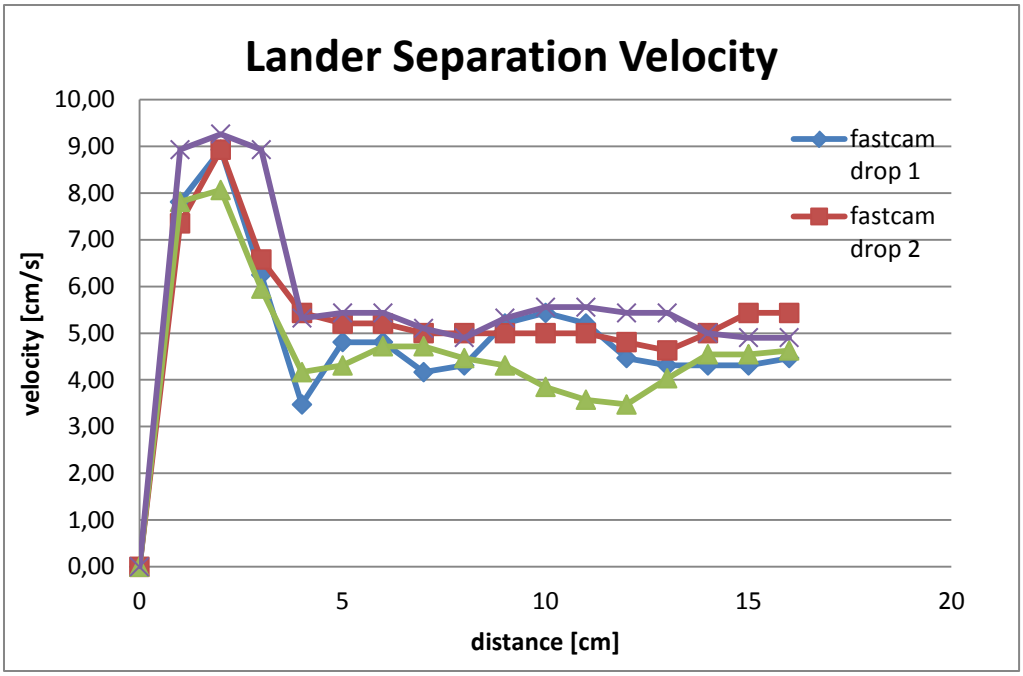

Figure 35: Separation velocity of the drop test campaign

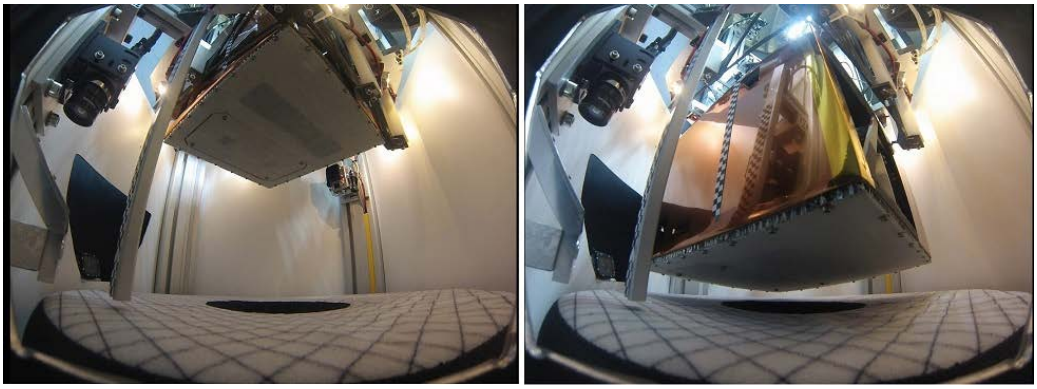

:

Figure 36: The separation recorded by the ProGo (bottom).